Biogeosciences, 21, 789–809, 2024
https://doi.org/10.5194/bg-21-789-2024

Biogeosciences Open Access EGU

Marine anoxia initiates giant sulfur-oxidizing bacterial mat proliferation and associated changes in benthic nitrogen, sulfur, and iron cycling in the Santa Barbara Basin, California Borderland

David J. Yousavich[1], De'Marcus Robinson[2], Xuefeng Peng[3], Sebastian J. E. Krause[1,4], Frank Wenzhöfer[5,6,7], Felix Janssen[5,6], Na Liu[8], Jonathan Tarn[8], Franklin Kinnaman[8], David L. Valentine[8], and Tina Treude[1,2]

[1]Department of Earth, Planetary, and Space Sciences, University of California, Los Angeles, 595 Charles E. Young Drive East, Los Angeles, CA 90095, USA
[2]Department of Atmospheric and Oceanic Sciences, University of California, Los Angeles, Math Science Building, 520 Portola Plaza, Los Angeles, CA 90095, USA
[3]School of Earth, Ocean, and Environment, University of South Carolina, 701 Sumter Street, Columbia, SC 29208, USA
[4]Earth Research Institute, 6832 Ellison Hall, University of California, Santa Barbara, CA 93106-3060, USA
[5]HGF-MPG Joint Research Group for Deep-Sea Ecology and Technology, Alfred Wegener Institute, Helmholtz Centre for Polar and Marine Research, Am Handelshafen 12, 27570 Bremerhaven, Germany
[6]HGF-MPG Joint Research Group for Deep-Sea Ecology and Technology, Max Planck Institute for Marine Microbiology, Celsiusstrasse 1, 28359 Bremen, Germany
[7]Department of Biology, HADAL center, University of Southern Denmark, 5230 Odense M, Denmark
[8]Department of Earth Science and Marine Science Institute, University of California, Santa Barbara, CA 93106, USA

Correspondence: David J. Yousavich (yousavdj@ucla.edu) and Tina Treude (ttreude@g.ucla.edu)

Received: 3 June 2023 – Discussion started: 19 June 2023
Revised: 14 December 2023 – Accepted: 18 December 2023 – Published: 14 February 2024

Abstract. The Santa Barbara Basin naturally experiences transient deoxygenation due to its unique geological setting in the southern California Borderland and seasonal changes in ocean currents. Long-term measurements of the basin showed that anoxic events and subsequent nitrate exhaustion in the bottom waters have been occurring more frequently and lasting longer over the past decade. One characteristic of the Santa Barbara Basin is the seasonal development of extensive mats of benthic nitrate-reducing sulfur-oxidizing bacteria, which are found at the sediment–water interface when the basin's bottom waters reach anoxia but still provide some nitrate. To assess the mat's impact on the benthic and pelagic redox environment, we collected biogeochemical sediment and benthic flux data in November 2019, after anoxia developed in the deepest waters of the basin and dissolved nitrate was depleted (down to 9.9 µM). We found that the development of mats was associated with a shift from denitrification to dissimilatory nitrate reduction to ammonium. The zone of sulfate reduction appeared near the sediment–water interface in sediment hosting these ephemeral white mats. We found that an exhaustion of iron oxides in the surface sediment was an additional prerequisite for mat proliferation. Our research further suggests that cycles of deoxygenation and reoxygenation of the benthic environment result in extremely high benthic fluxes of dissolved iron from the basin's sediment. This work expands our understanding of nitrate-reducing sulfur-oxidizing mats and their role in sustaining and potentially expanding marine anoxia.

1 Introduction

Naturally occurring low-oxygen waters in the ocean are commonly observed below the ocean's mixed layer where respiration consumes oxygen faster than it is produced or ventilated. When low-oxygen conditions occur along the western

continental shelf in regions susceptible to upwelling events and/or undergoing eutrophication, organic matter remineralization can frequently drive oxygen concentrations to hypoxic ($O_2 < 63\,\mu M$) (Middelburg and Levin, 2009) and/or anoxic ($O_2 < 3\,\mu M$) levels (Fossing et al., 1995; Canfield et al., 2010). These areas are usually referred to as oxygen minimum zones (OMZs). In the water column of OMZs, nitrogen reduction becomes an important mechanism for organic matter remineralization (Ward et al., 2009). OMZs within coastal basins that experience seasonal changes in upwelling can experience anoxic and nitrate-reducing conditions that extend to the benthic environment, especially when high productivity and associated organic matter export coincide with seasonal patterns of physical mixing. This fundamental change in the redox conditions at the sediment–water interface encourages elevated rates of anaerobic microbial processes and can promote organic matter preservation in the sediments (Middelburg and Levin, 2009; Treude, 2011), although a recent study has suggested that a thin reactive surface layer can provide high rates of organic matter degradation in anoxic environments (Van De Velde et al., 2023). Persistent anoxia in these coastal OMZs can lead to huge releases of sulfide (up to $13.7\,mmol\,m^{-2}\,d^{-1}$) and ammonium (up to $21.2\,mmol\,m^{-2}\,d^{-1}$) into the water column (Sommer et al., 2016).

The Santa Barbara Basin (SBB) is an example of one of these coastal OMZs that experiences seasonal deoxygenation. Drastic changes in water-column oxygenation and seafloor redox conditions drive complex changes in benthic biogeochemistry and microbiology, evidenced most clearly by the development of thick, expansive mats of giant sulfur-oxidizing bacteria (GSOB) on the SBB seafloor (Bernhard et al., 2003; Prokopenko et al., 2006; Valentine et al., 2016; Kuwabara et al., 1999). A 2013 survey of the basin identified a vast GSOB mat spread over 1.6 contiguous kilometers, confined between 487 and 523 m in the SBB depocenter where conditions were anoxic but not depleted of NO_3^- (Valentine et al., 2016). These GSOB mats have been noted previously in the SBB benthos, appearing at times of anoxia and disappearing when oxygen is present in the bottom water (Reimers et al., 1996; Kuwabara et al., 1999). Similar GSOB mats have been identified in other transiently deoxygenated OMZs such as the Peruvian and Chilean coast (Sommer et al., 2016; Schulz et al., 1996; Zopfi et al., 2001; Høgslund et al., 2009). The chemoautotrophic bacteria species that constitute the bulk of GSOB mats (typically *Thioploca* and/or *Beggiatoa*) utilize sulfide as an electron donor and O_2 or NO_3^- as a terminal electron acceptor (Jørgensen and Nelson, 2004). Some GSOB can hyper-accumulate NO_3^- in cell vacuoles up to 500 mM (Fossing et al., 1995) and use this NO_3^- reserve to oxidize sulfide that diffuses from the underlying sediment to perform their metabolism. (Huettel et al., 1996; Mußmann et al., 2003; Sayama, 2001).

The activity of GSOB mats contributes significantly to element cycling in benthic marine environments, with large effects on biogeochemical conditions in the bottom water. Isotopic measurements of $^{15}N/^{14}N$ and $^{18}O/^{16}O$ from NO_3^- in the SBB water column suggest that benthic organisms are responsible for approximately 75 % of the total NO_3^- reduction in the SBB (Sigman et al., 2003). Other studies have found that GSOB mats inhibit the diffusion of NO_3^- into sediments via hyper-accumulation in vacuoles, thereby creating conditions ideal for bacterial heterotrophic sulfate reduction beneath them (Fossing et al., 1995; Zopfi et al., 2001). These studies suggest that GSOB mats in the SBB may be responsible for the majority of NO_3^- consumption in the basin, rather than water-column microbes. Additionally, GSOB mats have been reported to deplete NO_3^- via dissimilatory nitrate reduction to ammonia (DNRA) in the anoxic bottom water of the Peruvian OMZ (Dale et al., 2016) and in the hypoxic transition zone in the eastern Gotland Basin of the Baltic Sea (Noffke et al., 2016). By contrast, benthic microbial communities in the hypoxic (42 µM) Mauritanian OMZ perform canonical denitrification instead (Dale et al., 2014). The contrast between the Peruvian and Mauritanian OMZs suggests that bottom-water anoxia triggers the appearance of GSOB mats and that DNRA is more prevalent where GSOB mats are present.

Rapid accumulation and consumption of NO_3^- by GSOB mats have ramifications for the redox conditions in the sediment underneath. The depletion of NO_3^- and shallowing of the nitracline could promote high rates of sulfate reduction in the sediment underneath the GSOB mat. In return, the sulfate reduction zone exists close to the sediment–water interface, providing the GSOB mat with readily accessible sulfide. If a metabolic feedback loop is then established between sulfur-oxidizing bacteria at the sediment–water interface and sulfate-reducing bacteria in the sediment, increased NO_3^- loss from the water column and spreading of sulfidic conditions in SBB sediment is expected. With these mats being potentially crucial to nitrogen and sulfur cycling in sediments underlying OMZs, their biogeochemical transformations and, ergo, effect upon basin redox conditions are critically important to understanding element cycling in the SBB. Such gained knowledge would have additional benefits for predicting biogeochemical feedbacks to the projected expansion of oceanic oxygen deficiency, in the SBB and in OMZs more generally, as a result of global change (Stramma et al., 2008).

Utilizing in situ technologies, sediment porewater extraction, solid-phase analyses, and radiotracer techniques, this study aims to answer the following overarching questions:

1. Which environmental conditions initiate and sustain the proliferation of GSOB mats?
2. Which biogeochemical transformations occur in the sediment underneath these mats?
3. What role do the mats play in the increasingly prevalent anoxic and nitrate-depleted condition found in the SBB?

These investigations represent the first basin-wide geochemical characterization of the Santa Barbara Basin, which hosts the largest (to date) mapped GSOB mat in the world's oceans. It is the first suite of in situ flux measurements carried out in the SBB, which is unique with respect to other heavily studied marine settings (e.g., the eastern Gotland Basin and Peruvian upwelling zone) in that it is an oceanic basin within an upwelling zone. The results presented here also provide a geochemical context for a number of other related investigations in the SBB (Robinson et al., 2024; Peng et al., 2023) as well as the first measurements in a multiyear study of biogeochemical changes in response to warming waters and increased stratification on the Californian coast.

2 Materials and methods

2.1 Study site

The Santa Barbara Basin (SBB) is a coastal basin in the California Borderland with an approximate maximum depth of 600 m characterized by a seasonally anoxic water column (Sverdrup and Allen, 1939; Sholkovitz and Gieskes, 1971). The transform boundary along the California Borderland heavily affects the geomorphology of basins in this region; these basins become twisted as the plates rub against each other and form a series of "bathtubs" blocked by sills and seamounts off the coast of California. The SBB is bordered by the California coast in the north, the Channel Islands in the south, the Santa Monica basin to the east, and the Arguello Canyon to the west. A sill to the west of the basin at around 475 m depth (Fig. 1) prohibits most water transfer between the Santa Lucia Slope and the deeper waters of the SBB (Sholkovitz and Gieskes, 1971). The highly productive surface waters in the basin provide ample organic matter to the basin's water column, encouraging strong remineralization processes below the euphotic zone, which can induce anoxia below the sill depth, with typically less than 1 $\mu mol\, O_2\, L^{-1}$ (Sholkovitz, 1973; Emery et al., 1962; Thunell, 1998; Emmer and Thunell, 2000). Benthic faunal distribution within the basin is tightly correlated with this sill depth and the related oxygen conditions; below the sill, the sea snail *Alia permodesta* is the most commonly found benthic fauna, while sea stars, sea urchins, and other echinoderms increase in density above the sill (Myhre et al., 2018). During upwelling events (usually in spring), oxygenated waters from the California Current spill over the western sill and ventilate the SBB, reportedly increasing bottom-water oxygen concentrations to approximately 20 $\mu mol\, O_2\, L^{-1}$ (Goericke et al., 2015). SBB water-column oxygen and nitrogen concentrations have been evaluated through a longitudinal survey by the California Cooperative Oceanic Fisheries Investigations (CalCOFI), with data starting in the 1950s. The data collected by this survey show increasing durations of anoxia and fixed nitrogen loss in the basin, with the SBB becoming completely nitrate-depleted below the sill at least three times between 2012 and 2017 (https://calcofi.org/data/, last access: 26 January 2024).

2.2 Benthic sediment sampling and instrument deployment

Sediment samples were taken between 30 October and 11 November 2019 during an expedition aboard the research vessel (R/V) *Atlantis* equipped with the remotely operated vehicle (ROV) *Jason*. Samples were taken at stations along a bimodal, north–south transect through the depocenter of the SBB as well as at one station on a separate transect. Details of sampling stations can be seen in Fig. 1a and b. Briefly, depocenter stations are labeled as NDRO and SDRO (northern and southern depocenter radial origin, respectively). The remaining stations are named for the cardinal direction (north vs. south) and the transect number (e.g., SDT1-A is on transect 1, while SDT3-A is on transect 3). As station depth decreases, the alpha suffix increases (e.g., NDT3-A is deeper than NDT3-B, etc.).

The ROV *Jason* conducted sediment push coring and deployed automated benthic flux chambers (BFCs) and microprofilers at each station. Bottom-water oxygen concentration was determined using an Aanderaa 4831 oxygen optode (Aanderaa Instruments, Bergen, Norway) installed on the ROV. Optical modems (Luma 250LP, Hydromea, Renens, Switzerland) installed on the ROV and the BFCs and microprofilers were used to transmit deployment settings and start/terminate measurements of the instruments. Multiple push cores (polycarbonate, 30.5 cm length, 6.35 cm inner diameter) per sampling station were retrieved during ROV *Jason* deployments (Fig. 1c). Replicate cores from each station were transferred to an onboard 6 °C cold room upon recovery aboard the ship and subsampled for either solid-phase analyses, porewater geochemistry, or radiotracer experiments.

2.3 Sediment core subsampling

Two replicate ROV push cores that were collected near each other at each station were processed under a constant argon flow to protect redox-sensitive species. Cores were sectioned in 1 cm increments up to 10 cm followed by 2 cm increments. Note that sediments from the NDT3-B station were sliced in 2 cm increments. Sediment subsections were transferred into argon-filled 50 mL conical centrifuge tubes. Sediment samples were centrifuged at $2300 \times g$ for 20 min. The centrifugate was subsampled unfiltered as fast as possible (to avoid contamination with oxygen) for porewater analyses. Solid-phase cores were sectioned similar to porewater cores and subsampled for sediment density, porosity, and organic matter content. A 10 mL cutoff plastic syringe was used to collect 6 mL of sediment into pre-weighed plastic vials (15 mL snap-cap vials) and stored in the dark at 4 °C for sediment porosity and density analysis. Next, 2 mL microcentrifuge tubes were filled with sediment from each depth interval and

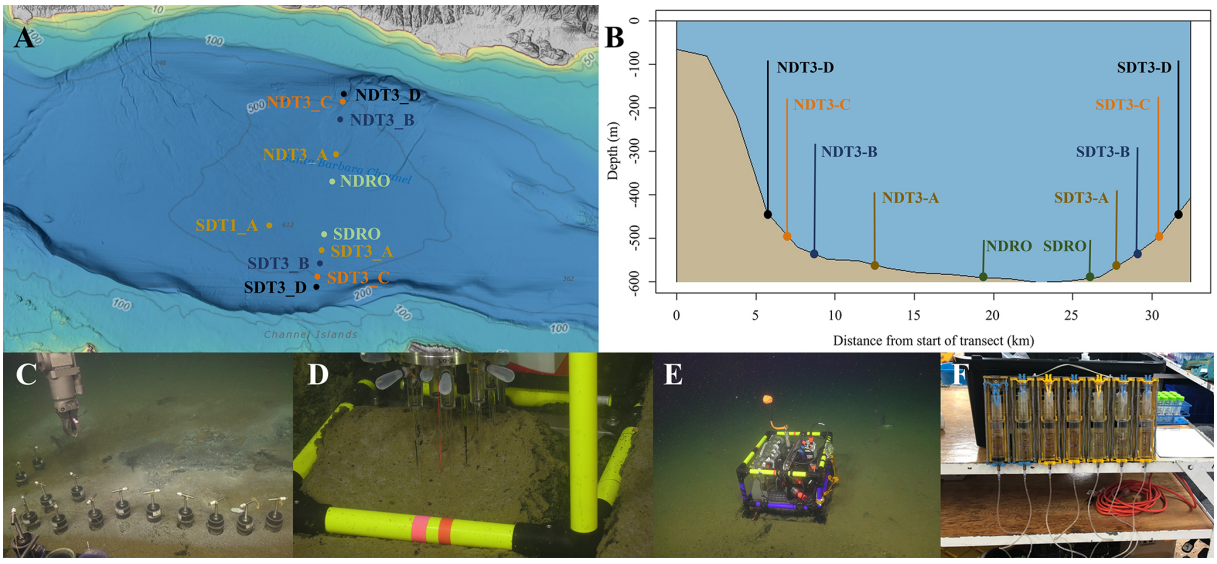

Figure 1. Maps of sampling locations in the Santa Barbara Basin and photographs of deployed equipment: **(a)** bathymetric map of the Santa Barbara Basin with locations of all sampled stations; **(b)** cross section of the Santa Barbara Basin with locations of all sampled stations; **(c)** sediment push coring with the ROV arm; **(d)** sediment microprofiler; **(e)** benthic flux chamber; (*F*) a close-up of a syringe system from a benthic flux chamber. The map in panel **(a)** was generated using the Bathymetric Data Viewer provided by the National Centers for Environmental Information.

stored at −30 °C for sediment organic matter analyses. One ROV push core per station was subsampled with a miniaturized push core (length 20 cm, inner diameter 2.6 cm) and taken immediately to the shipboard radioisotope van for radiotracer experiments (see Sect. 2.5).

2.4 Sediment porewater geochemistry

Concentrations of porewater sulfide (Cline, 1969), NH_4^+, PO_4^{3-}, and Fe^{2+} (Grasshoff et al., 1999) were determined shipboard with a Shimadzu UV-Vis spectrophotometer (UV-1800). Detection limits for sulfide, NH_4^+, PO_4^{3-}, and Fe^{2+} were 1 µM. Subsamples (2 mL) for porewater NO_3^- and NO_2^- concentrations were stored in 2 mL plastic vials with an O-ring, frozen shipboard at −30 °C, and analyzed back at the home laboratory on the same spectrophotometer using the method following García-Robledo et al. (2014). The detection limit for NO_3^- and NO_2^- was 0.5 µM. Samples for porewater dissolved inorganic carbon (DIC) were preserved shipboard with 5 µL saturated HgCl in headspace-free glass vials and stored at 4 °C for later analysis following Hall and Aller (1992). The DIC detection limit was 0.1 mM. Total alkalinity was determined shipboard using direct titration of 500 µL of porewater with 0.01 M Titrisol® HCl (Pavlova et al., 2008). The analysis was calibrated using a International Association for the Physical Sciences of the Oceans (IAPSO) seawater standard, with a precision and detection limit of 0.05 meq L^{-1}. Subsamples (1 mL) for sulfate and chlorinity were stored in 2 mL plastic vials with an O-ring, frozen shipboard at −30 °C, and later measured in the lab using a Metrohm 761 ion chromatograph with a methodological detection limit of 30 µM (Dale et al., 2015).

2.5 Solid-phase analyses

Porosity and density samples were collected in pre-weighed plastic vials and dried at 50 °C for up to 96 h until the dry weight was stable. Sediment porosity was calculated by taking the difference between the wet and dry sediment weight and dividing it by the volume of the wet sediment. Sediment density was calculated by dividing the wet sediment weight by its volume. The treatment of sediment subsamples for total organic carbon (TOC), total organic nitrogen (TON), and organic carbon isotope composition ($\delta^{13}C$) was modified from Harris et al. (2001), and subsamples were sent to the UC Davis Stable Isotope Facility for analysis using elemental analyzer–isotope ratio mass spectrometry. TOC and TON were calculated based on the sample peak area corrected against a reference material (alfalfa flour). The limit of quantification based on peak area was 100 µg C with an uncertainty of ±0.2 ‰ for $\delta^{13}C$.

2.6 Sulfate reduction

To determine ex situ microbial sulfate reduction rates, whole round sub-cores were injected with 10 µL carrier-free ^{35}S-sulfate radiotracer (dissolved in water, 200 kBq, specific activity of 37 TBq $mmol^{-1}$) into pre-drilled, silicon-filled holes at 1 cm increments according to Jørgensen (1978). These sub-cores were incubated at 6 °C in the dark for 6–8 h. Incubations were stopped by slicing sediment cores in 1 cm

increments into 50 mL centrifuge tubes filled with 20 mL zinc acetate (20 % w/w) that were then frozen at −20 °C until analysis in the land-based laboratory. Microbial activity in controls was terminated with zinc acetate (20 mL of 20 % w/w) before the addition of radiotracer and subsequent freezing. Lab-based analysis of sulfate reduction rates were determined following the cold-chromium distillation procedure (Kallmeyer et al., 2004).

2.7 Benthic in situ investigations

Per station, one to three microprofiler (Fig. 1d) and three BFC (Fig. 1e) deployments were carried out by the ROV *Jason* at the seafloor. Construction, deployment, and operation of automated microprofilers and BFCs followed those described in Treude et al. (2009). The microprofiler deployed in this study represents a modified, miniaturized version of the instrument described in Gundersen and Jørgensen (1990) that was constructed specifically for use by an ROV. Microprofilers were outfitted with three O_2 microelectrodes (Glud et al., 2000), two pH microelectrodes (Revsbech and Jørgensen, 1986), two H_2S microelectrodes (Jeroschewsky et al., 1996), and one conductivity sensor to determine the position of the sediment–water interface relative to the tips of the microelectrodes. Concentrations of oxygen and sulfide as well as the pH were each calculated from microelectrode readings and averaged for the respective sites where replicates existed.

The BFCs consisted of a frame equipped with a cylindrical polycarbonate chamber (inner diameter = 19 cm) with its lower portion sticking out of the frame. The upper side of the chamber was closed by a lid containing a stirrer (Type K/MT 11, K.U.M., Kiel, Germany), oxygen optodes (Type 4330, Aanderaa Data Instruments, Bergen Norway and HydroFlash, Contros/Kongsberg Maritime, Kongsberg, Norway), a conductivity sensor (type 5860, Aanderaa Data Instruments), and a valve. Prior to insertion into the sediments, the chambers were held upside down by the ROV manipulating arms within approximately 10 m of the seafloor and moved back and forth to make sure that water from shallower depths that may have been trapped was replaced by bottom water. Chamber incubations lasted between 240 and 390 min. Each BFC was outfitted with a custom-built syringe sampler containing seven syringes that were connected by tubes to sampling ports in the upper wall of the chambers (Fig. 1f): one injection syringe and six sampling syringes that were fired at regular time intervals over the time course of the deployment. The injection syringe contained deionized water, and the reduction in salinity in the overlying water after salinity readings stabilized (i.e., full mixing was achieved) 10–30 min after injection was used to determine BFC volumes (Kononets et al., 2021). Samples obtained from the overlying water of the BFC were examined for the same geochemical constituents as described above (Sect. 2.4). Benthic fluxes of NO_3^-, NH_4^+, PO_4^{3-}, and Fe^{2+} were calculated as follows:

$$J = \frac{\Delta C}{\Delta t} \cdot \frac{V}{A}, \quad (1)$$

where J is the flux (in mmol m^{-2} d^{-1}), ΔC is the concentration change (in mmol m^{-3}), Δt is the time interval (in d), V is the overlying water volume (in m^3), and A is the surface area of the sediment covered by the benthic flux chamber (in m^2). An average flux within the BFCs was calculated for stations of similar depth. One chamber per site contained ^{15}N-NO_3^- in the injection syringe for in situ nitrogen-cycling experiments. Results are reported from two of these chambers (SDRO and NDT3-D), and all ^{15}N-NO_3^- chambers were excluded from benthic flux calculations (see next section).

2.8 In situ ^{15}N incubations

A total of 200 µmol of ^{15}N-labeled potassium nitrate (99 % ^{15}N; Cambridge Isotopes) was injected into the ^{15}N incubation chamber at each site to obtain a final concentration of ∼ 50–100 µM of ^{15}N-labeled nitrate. Nitrate was amended at this level to prevent its depletion before the last sampling time point (Valentine et al., 2016). Samples for $\delta^{15}N$ analysis were preserved by filling a pre-vacuumed 12 mL Exetainer vial with 0.1 mL 7M zinc chloride as a preservative. Another aliquot (∼ 12 mL) of seawater for ammonium isotope analysis (see Sect. 2.7.2) was filtered through 0.2 µm syringe filters and stored frozen. Prior to analyzing the samples in 12 mL Exetainer vials, 5 mL of sample was replaced with ultrahigh-purity helium to create a headspace. The concentration and $\delta^{15}N$ of dissolved N_2 and N_2O were determined using a Sercon CryoPrep gas concentration system interfaced to a Sercon 20-20 isotope ratio mass spectrometer (IRMS) at the UC Davis Stable Isotope Facility.

2.9 Ammonium isotope analyses

The production of $^{15}NH_4^+$ in seawater samples was measured using a method adapted from Zhang et al. (2007) and described previously by Peng et al. (2016). In brief, NH_4^+ was first oxidized to NO_2^- using hypobromite (BrO^-) and then reduced to N_2O using an acetic acid–azide working solution (Zhang et al., 2007). The $\delta^{15}N$ of the produced N_2O was determined using an Elementar Americas PrecisION continuous flow multicollector isotope ratio mass spectrometer coupled to an automated gas extraction system as described in Charoenpong et al. (2014). Calibration and correction were performed as described in Bourbonnais et al. (2017). The measurement precision was ±0.2 ‰ for $\delta^{15}N$. Depending on the in situ ammonium concentration, the detection limit for total NH_4^+ production rates ranged between 0.006 and 0.0685 mmol m^{-2} d^{-1}.

Table 1. Station details and photos of representative ROV push cores taken at each station. Mat presence (Y: yes; N: no) was determined visually. Station water depth and oxygen concentration were determined by sensors attached to ROV *Jason* (bdl: below detection limit, $< 3\,\mu M$ O_2). Anoxia was confirmed by additional methods (see discussion in Sect. 4.1). Latitude and longitude were determined by triangulation between the ROV and the ship. Bottom-water nitrate concentration was derived from an average of benthic flux chamber nitrate measurements at time 0 for each station (chambers with no calculable flux and ^{15}N-nitrate addition excluded). Note that benthic flux chambers were not deployed at SDT1-A. Photographs show the sediment–water interface (SWI; top part) and each sediment core in full length (lower part).

Parameter	NDT3-D	NDT3-C	NDT3-B	NDT3-A	NDRO	SDRO	SDT1-A	SDT3-A	SDT3-B	SDT3-C	SDT3-D
Mat Present	N	N	N	Y	Y	Y	Y	Y	N	N	N
Depth (m)	447	498	537	572	580	586	573	571	536	494	447
Latitude (°)	34.363	34.353	34.333	34.292	34.262	34.201	34.212	34.184	34.168	34.152	34.142
Longitude (°)	-120.015	-120.016	-120.019	-120.026	-120.031	-120.044	-120.116	-120.047	-120.053	-120.050	-120.052
Oxygen (µM)	8.7	5.2	12.2	9.2	0.0	0.0	0.0	0.0	1.8	3.1	9.6
Nitrate (µM)	27.3	26.0	11.5	24.4	18.5	9.9		20.4	20.6	16.3	28.0

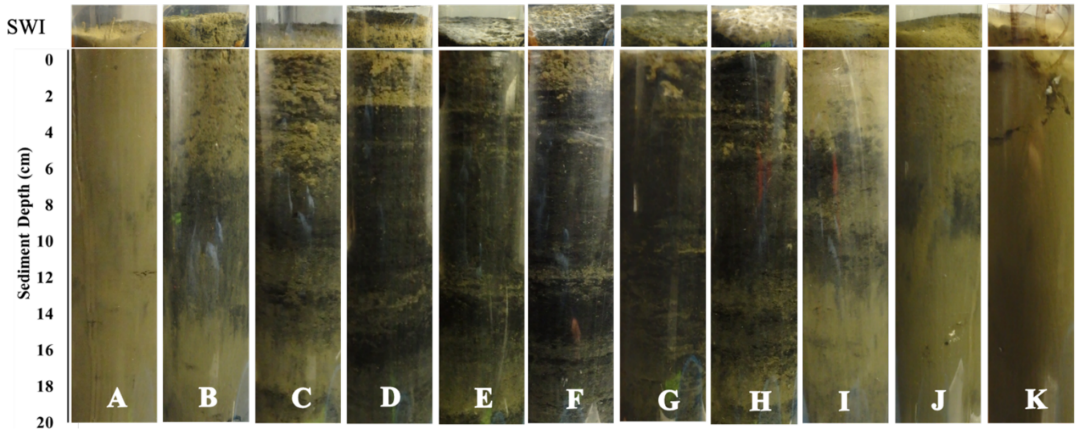

3 Results

3.1 Bottom-water conditions

O_2 and NO_3^- concentrations in the bottom water along the transects can be seen in Table 1. O_2 concentrations below detection as determined by the ROV sensor could, in some cases, be considered to represent anoxia ($0\,\mu M$ O_2) based on a set of different analytical methods (see discussion in Sect. 4.1). Bottom-water solute concentrations (as defined by the average T_0 concentration in BFCs at each site) can be seen in Figs. S1–S4 in the Supplement. Bottom-water NO_3^- concentrations roughly decreased with station depth (e.g., 28 µM at NDT3-D vs. 19 µM at NDRO). Bottom-water NO_2^- concentrations were below detection at all stations. Bottom-water NH_4^+ concentrations were 9 µM at NDRO, 13 µM at SDRO, and below detection at shallower stations. Bottom-water PO_4^{3-} concentrations roughly increased with increasing basin depth (e.g., 2 µM at SDT3-D vs. 7 µM at SDRO). Finally, Fe^{2+} was 2 and 5 µM at the NDRO and SDRO stations, respectively, whereas it was below detection at all shallower stations.

3.2 Sediment characteristics

Photographs of sediment cores with a depth scale are shown below Table 1. Sediment colors were classified according to Hossain et al. (2014). Cores from the shallowest (D) stations were uniformly reddish in color with small pockets of black. The sediment color changed with station depth, transitioning from a reddish color at the shallowest stations to predominantly black with reddish laminations at the depocenter stations. The band of black sediment appeared at approx. 8 cm sediment depth in the C-station cores and became progressively more ubiquitous with station depth. Notably, NDT3-C sediment (Table 1b) contained black bands from approx. 6–14 cm sediment depth, while SDT3-C sediment (Table 1j) had a much narrower band around 8–10 cm. Sediment cores from shallower stations (D and C stations) contained signs of bioturbation (e.g., U-shaped burrows) and, in some cases, contained visible macrofauna, such as polychaetes and mollusks. Deeper in the basin (A and depocenter stations), no signs of bioturbation were detected and the sediment–water interface was colonized by patches of white GSOB mats. Spherical cells (given the moniker "ghost balls") were found mixed amongst giant sulfur bacteria filaments within the top 0–1 cm of sediment at NDRO (Fig. S7). These unknown species had similar morphological characteristics to the species *Thiomargarita namibiensis* (Schulz et al., 1999; Schulz and Schulz, 2005), containing a translucent cell with sulfur granules that gave them a ghostly white appearance. A small sample of cells ($n = 8$) were measured, featuring diameters between 48.0 and 99.6 µm, amounting to an average biovolume of $2.5 \times 10^5\,\mu m^3$, compared with *T. namibiensis* with a cell diameter usually between 100 and 300 µm (Schulz

et al., 1999). B-station cores contained sporadic GSOB filaments slightly deeper in the sediment (approx. 2–4 cm sediment depth). Sediment solid-phase parameters (averaged over the entire sediment core depth) can be seen in Table 2. Average sediment porosity increased with basin depth (e.g., from 0.79 at NDT3-D to 0.88 at NDRO). TOC, TON, the C/N ratio, and the $\delta^{13}C$ isotopic signature of organic carbon remained relatively constant (2.5 %–4.5 %, 0.1 %–0.4 %, 8.0 %–8.7 %, and 21.3 %–22.4 %, respectively) over all stations.

3.3 Sediment porewater geochemistry

Total alkalinity (Figs. 2a–e, 3a–f) increased steadily with sediment depth at all stations starting with, on average, 2.4 mM in the core supernatant and reaching a maximum at the respective deepest sediment sample (20 cm). Porewater alkalinity and DIC also increased with basin depth (Figs. 2a–e, 3a–f), indicating that total alkalinity was dominated by the carbonate system. Porewater DIC was, on average, 2.2 mM in the core supernatant and reached maximum concentrations at the deepest sediment depth (20 cm) at most stations.

Porewater PO_4^{3-} profiles (Figs. 2a–e, 3a–f) were markedly different between the depocenter and shallower C and D stations. Porewater PO_4^{3-} concentrations in the depocenter and A stations generally increased with sediment depth, but several profiles (NDT3-C, NDT3-A, SDRO, and SDT1-A) remained unchanged or decreased deeper in the sediment (starting at approx. 10 cm). The profiles at the C and D stations showed a peak in PO_4^{3-} concentrations near the sediment–water interface, particularly in the northern basin. Below 2 cm, PO_4^{3-} decreased with sediment depth, but it sometimes showed a second small peak deeper in the sediment (12–14 cm at NDT3-D and 10–12 cm at SDT3-D).

Porewater NH_4^+ concentrations (Figs. 2a–e, 3a–f) showed trends that were often similar to alkalinity and DIC; NH_4^+ concentrations increased downcore and were higher at the depocenter than at D stations (e.g., 370 and 91 µM at 20 cm for SDRO and SDT3-D, respectively). Porewater NO_2^- (Table S1 in the Supplement) and NO_3^- (Figs. 2f–j, 3g–l) concentrations were at or near zero below 2 cm at every station except for SDRO and NDT3-A, where large peaks in NO_3^- (376 and 81 µM, respectively) and NO_2^- (37 and 5 µM, respectively) occurred in the top 1 cm.

Porewater Fe^{2+} concentrations (Figs. 2f–j, 3g–l) were several orders of magnitude higher at shallower D stations (max values of 722 and 395 µM at NDT3-D and SDT3-D, respectively) compared with depocenter stations (max values of 13 and 51 µM at NDRO and SDRO, respectively). The NDT3-C porewater Fe^{2+} concentration (Fig. 2g) peaked in the top 1 cm of sediment (similar to deeper stations), while the SDT3-C porewater Fe^{2+} concentration (Fig. 3h) peaked at around 5 cm sediment depth. Fe^{2+} concentrations reached a maximum at 0–2 cm and declined sharply with depth in the depocenter and A-station sediment. Northern basin sediment was similar, but the decline in Fe^{2+} below 0–2 cm was less pronounced.

Maximum porewater sulfide concentrations (Figs. 2f–j, 3g–l) were several orders of magnitude lower at the shallower D stations (5 and 4 µM at NDT3-D and SDT3-D, respectively) compared with the A stations (350 and 148 µM at NDT3-A and SDT1-A, respectively). Unlike Fe^{2+}, peaks in sulfide concentration occurred deeper in the sediment (e.g., below 5 cm depth at A stations). Porewater sulfate concentrations (Figs. 2k–o, 3m–r) decreased slightly with depth, but they never reached values below 20 mM at any station.

3.4 In situ microprofiling

Microprofiler O_2 and sulfide measurements are shown in Fig. 4. Oxygen was rapidly consumed within the first 0–1 cm of sediment at every station at which O_2 was detected in the bottom water (i.e., at all stations except NDRO, which showed no positive signal of oxygen in the water compared to the sediment; note that no oxygen profile is available for SDRO). Sulfide concentrations from microsensors showed similar trends to spectrophotometric measurements, albeit with different absolute values (below detection in the shallower B, C, and D stations that lacked mats and > 1000 µM at the A and depocenter stations). Microprofiler pH (Fig. 4) was near 7.5 in the bottom water at all stations and slowly decreased to near 7.0 in the lower parts (3–5 cm) of the sediment at most stations except at NDT3-C and SDT3-B. The pH at 2.5 cm at SDT3-B reached 6.77, which was the lowest observed during this expedition.

3.5 In situ fluxes of benthic solutes

NO_3^-, NH_4^+, PO_4^{3-}, and Fe^{2+} flux measured in the BFCs revealed different patterns of uptake and release from the sediment throughout the basin (Figs. 5, S1–S4). BFC O_2 concentrations were compromised by O_2 release from the chamber's polycarbonate walls, which prevented an accurate calculation of O_2 fluxes from BFC sensor data. NO_3^- was consumed at all stations, as indicated by a negative flux (i.e., a flux into the sediment). On the contrary, benthic release (i.e., a flux out of the sediment) was observed for all other analyzed solutes (NH_4^+, PO_4^{3-}, and Fe^{2+}), with the lowest fluxes at the shallow D and C stations and the highest fluxes at the depocenter. Ammonium fluxes were the highest of all the determined solutes and showed the largest difference between deep and shallow stations, with a flux of 1.6 mmol m^{-2} d^{-1} at NDT3-C (there were no measurable NH_4^+ fluxes in D-station chambers) and up to 11.1 ± 3.1 mmol m^{-2} d^{-1} ($n = 3$) at the two depocenter stations. The depocenter ammonium flux far outpaced the concomitant flux of nitrate into depocenter sediments (-3.2 ± 0.7 mmol m^{-2} d^{-1}, $n = 3$). Iron and phosphate fluxes were similar at depocenter stations (4.1 ± 0.7, $n = 3$, and 3.2 ± 0.7, $n = 3$ mmol m^{-2} d^{-1}, respectively). Alkalinity and DIC concentrations from flux

Table 2. Sediment solid-phase data: porosity, density, total organic carbon (TOC), total organic nitrogen (TON), C : N ratio, and $\delta^{13}C$. All data were averaged for the top 0–19 cm of sediment except for NDT3-C (17 cm), NDT3-A (11 cm), and SDRO (7 cm), where the core length was shorter. The integrated sulfate reduction rate (SRR) values were integrated over a 0–14 cm sediment depth. No sulfate reduction rates are available for NDT3-B, SDT3-A, or SDT3-B; rates were not integrated for SDRO due to missing surface samples.

Station	Porosity	Density	TOC (%)	TON (%)	C : N ratio	$\delta^{13}C$ (‰)	Integrated SRR (mmol m^{-2} d^{-2})
NDT3-D	0.79 ± 0.03	1.21 ± 0.07	2.9 ± 0.5	0.3 ± 0.1	8.9 ± 0.2	-22.4 ± 0.3	2.9
NDT3-C	0.81 ± 0.04	1.16 ± 0.08	2.5 ± 0.5	0.5 ± 0.1	8.7 ± 0.5	-22.4 ± 0.4	3.8
NDT3-B	0.86 ± 0.04	1.06 ± 0.08	3.6 ± 0.5	0.4 ± 0.1	8.5 ± 0.5	-22.2 ± 0.4	
NDT3-A	0.88 ± 0.03	1.05 ± 0.04	3.1 ± 0.4	0.4 ± 0.1	8.2 ± 0.2	-22.1 ± 0.2	2.7
NDRO	0.88 ± 0.04	1.06 ± 0.03	3.3 ± 0.4	0.4 ± 0.0	8.2 ± 0.4	-22.1 ± 0.2	4.1
SDRO	0.87 ± 0.03	1.04 ± 0.03	3.5 ± 0.4	0.4 ± 0.1	8.0 ± 0.2	-22.0 ± 0.3	
SDT1-A	0.88 ± 0.03	1.11 ± 0.23	4.5 ± 0.5	1.0 ± 0.1	8.6 ± 0.8	-21.3 ± 0.7	2.9
SDT3-A	0.86 ± 0.04	1.05 ± 0.05	3.2 ± 0.0	0.4 ± 0.0	8.3 ± 0.6	-22.1 ± 0.4	
SDT3-B	0.85 ± 0.04	1.12 ± 0.06	3.6 ± 0.6	0.4 ± 0.1	8.3 ± 0.3	-22.0 ± 0.2	
SDT3-C	0.82 ± 0.04	1.22 ± 0.05	3.6 ± 0.8	0.4 ± 0.1	8.7 ± 0.3	-21.9 ± 0.2	1.7
SDT3-D	0.78 ± 0.04	1.22 ± 0.03	3.3 ± 0.5	0.4 ± 0.1	8.5 ± 0.2	-22.0 ± 0.1	1.9

chambers (Figs. S5, S6) remained constant at all stations; thus, no DIC flux was calculated. Results from BFCs injected with $^{15}N\text{-}NO_3^-$ at the SDRO and NDT3-D stations are shown in Fig. 6. The rates of denitrification, anammox, and N_2O production were higher at SDRO compared with NDT3-D. The $^{15}NH_4^+$ production (DNRA) was 1 order of magnitude higher at the SDRO station (2.67 mmol m^{-2} d^{-1}) compared with the NDT3-D station (0.14 mmol m^{-2} d^{-1}). DNRA accounted for a much higher percentage of NO_3^- reduction at SDRO (54.1 %) than at NDT3-D (13.3 %).

3.6 Sulfate reduction rates

Vertical profiles of bacterial sulfate reduction, as determined using the radioisotope technique, differed throughout the basin (Figs. 2k–o, 3m–r). Peaks in sulfate reduction were seen in the top 0–1 cm of sediment at stations with a visible GSOB mat on the surface (120.2, 151.0, and 85.3 nmol cm^{-3} d^{-1} at NDRO, SDT1-A, and NDT3-A, respectively). Sediments at most shallower basin depths exhibited peaks slightly deeper in the sediment and of lower magnitude (25.5, 44.5, and 22.5 nmol cm^{-3} d^{-1} at SDT3-C, NDT3-D, and SDT3-D, respectively). NDT3-C had no visible GSOB mats but exhibited a peak (133.7 nmol cm^{-3} d^{-1}) in sulfate reduction at 0–1 cm depth, similar to deeper stations (e.g., NDRO in Fig. 2o), which differed from other shallow stations (e.g., SDT3-C in Fig. 3n). The integrated sulfate reduction rate (0–14 cm depth) at NDRO (4.1 mmol m^{-2} d^{-1}) was noticeably higher than most other stations with the exception of NDT3-C (3.8 mmol m^{-2} d^{-1}) (Table 2). NDT3-D and NDT3-C exhibited higher integrated rates (2.9 and 3.8 mmol m^{-2} d^{-1}, respectively) than their southern station counterparts SDT3-D and SDT3-C (1.9 and 1.7 mmol m^{-2} d^{-1}, respectively).

4 Discussion

4.1 Giant sulfur-oxidizing bacterial mats proliferated in response to deoxygenation in the Santa Barbara Basin

The SBB is an ideal environment to study the effect of transient deoxygenation on benthic biogeochemistry. In fall 2019, when this expedition took place, the SBB was undergoing a transition from oxygenated to virtually anoxic conditions (Qin et al., 2022). When the AT42-19 cruise occurred, most of the bottom water in the basin was hypoxic (A, B, C, and D stations) except for the depositional center. Separate O_2 measurements from the ROV sensor (O_2 below the detection limit; Table 1), microprofilers (no signal change between the water column and sediment; Fig. 4), and Winkler titration from CTD/rosette casts (uniform non-zero value below 500 m (Qin et al., 2022)) indicated full anoxia in the bottom water at the deeper stations (NDRO and SDRO). Notably, bottom-water conditions revealed a slight asymmetry between the basin transects (Fig. 1): bottom water along the northern transect generally had more O_2 and NO_3^- than the southern transect (e.g., 9 µM O_2 at NDT3-A and 0 µM O_2 at SDT3-A). This asymmetry indicated differences in the circulation and/or microbial communities between the northern and southern portions of the basin. Whether this asymmetry is a permanent feature of the basin or symptomatic of the specific conditions in November 2019 is unclear; previous studies in the SBB have been restricted to the depocenter or one side of the basin (Sholkovitz, 1973; Reimers et al., 1996; Kuwabara et al., 1999). Regardless of bottom-water oxidant concentration, the energetically most favorable terminal electron acceptors (O_2 and NO_3^-) disappeared in a very narrow zone below the sediment–water interface, consistent

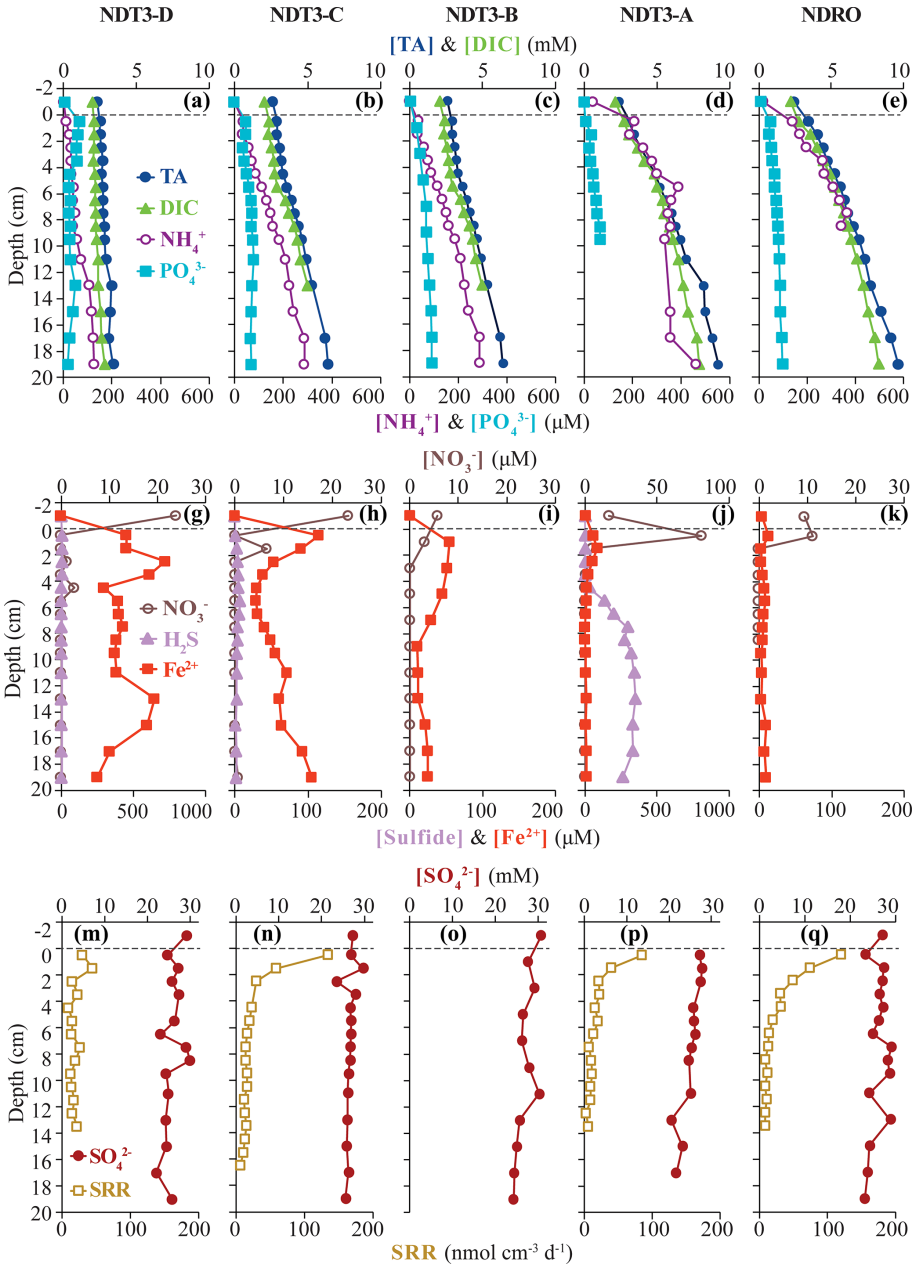

Figure 2. Biogeochemical data from ROV sediment push cores collected at stations on the northern transect (NDT3) and in the northern depocenter (NDRO): total alkalinity (TA), dissolved inorganic carbon (DIC), ammonium (NH_4^+), and phosphate (PO_4^{3-}) in the first row; nitrate (NO_3^-), total sulfide (sulfide), and iron (II) (Fe^{2+}) in the second row; and sulfate (SO_4^{2-}) and bacterial sulfate reduction rate (SRR) in the third row. Data analyzed from sediment core supernatant are plotted at a −1 cm sediment depth; the dotted line connotes the sediment–water interface. Note the change in scale on the primary x axis in panel **(i)** and the change in scale on the secondary x axis in **(f)** and **(i)**. No spectrophotometric sulfide data are available for NDRO and NDT3-B, and no SRR data are available for NDT3-B. For station details, see Fig. 1 and Table 1.

with their expected rapid consumption by the benthic microbial community.

In the present study, benthic GSOB mats were primarily limited to the anoxic depocenter of the SBB. Similarly, such mats were replete in the core of the anoxic Peruvian OMZ (Levin et al., 2002; Sommer et al., 2016; Mosch et al., 2012) but absent from the seafloor below the hypoxic, i.e., slightly oxygenated, Mauritanian OMZ (Schroller-Lomnitz et al., 2019). GSOB mats in November 2019 were observed deeper in the basin than in October 2013 (Valentine et al.,

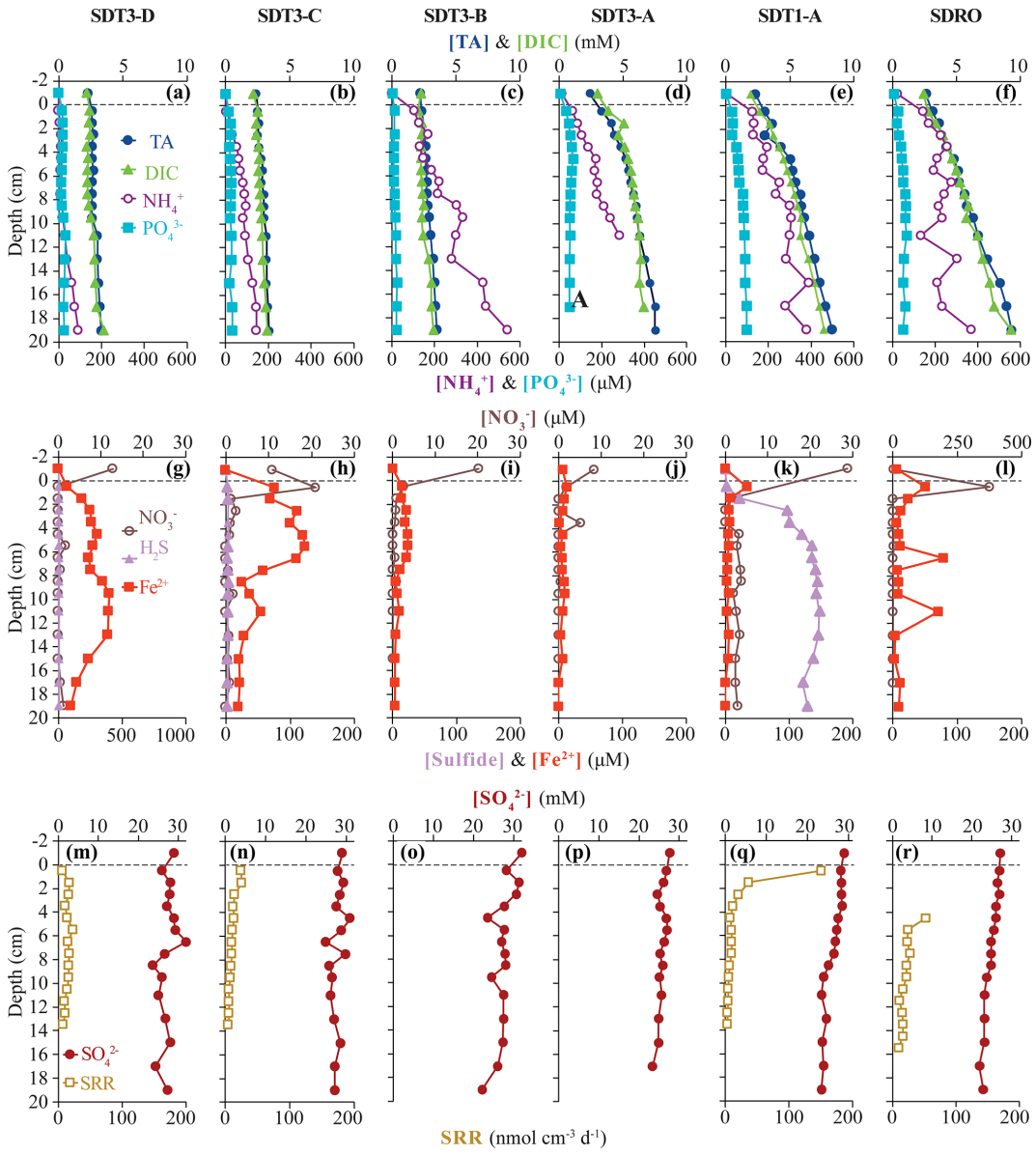

Figure 3. Biogeochemical data from ROV sediment push cores collected at stations on the two southern transects (SDT1 and SDT3) and the southern depocenter (SDRO): total alkalinity (TA), dissolved inorganic carbon (DIC), ammonium (NH_4^+), and phosphate (PO_4^{3-}) in the first row; nitrate (NO_3^-), total sulfide (sulfide), and iron (II) (Fe^{2+}) in the second row; and sulfate (SO_4^{2-}) and bacterial sulfate reduction rate (SRR) in the third row. Data analyzed from sediment core supernatant are plotted at a −1 cm sediment depth; the dotted line connotes the sediment–water interface. Note the change in scale on the primary x axis in **(l)** and the change in scale on the secondary x axis in **(g)**. No sulfide nor SRR data are available for SDT3-B and -A; spectrophotometric sulfide and the top 0–4 cm of SRR data are not available for SDRO. For station details, see Fig. 1 and Table 1.

2016) but in a similar location to June 1988 (Reimers et al., 1996) and April 1997 (Kuwabara et al., 1999). During the 2013 sampling, dense GSOB mats were confined to depths between approx. 500 and 570 m (equivalent to the B stations from this expedition), corresponding to anoxic conditions in the bottom water. This habitat was sandwiched between an anoxic, anitric (i.e., nitrate-free) deep water layer and a hypoxic, nitrogenated (i.e., nitrate-rich) shallower water layer (Valentine et al., 2016). The difference in depth distribution of GSOB mats between the 2013 and 2019 expeditions provides evidence that GSOB mats in the SBB are ephemeral and proliferate where the bottom water is anoxic but not anitric.

As our study represents only a snapshot of an oxygen- and nitrate-driven mat dynamic, we can only speculate regarding how areas of the basin that did not contain GSOB

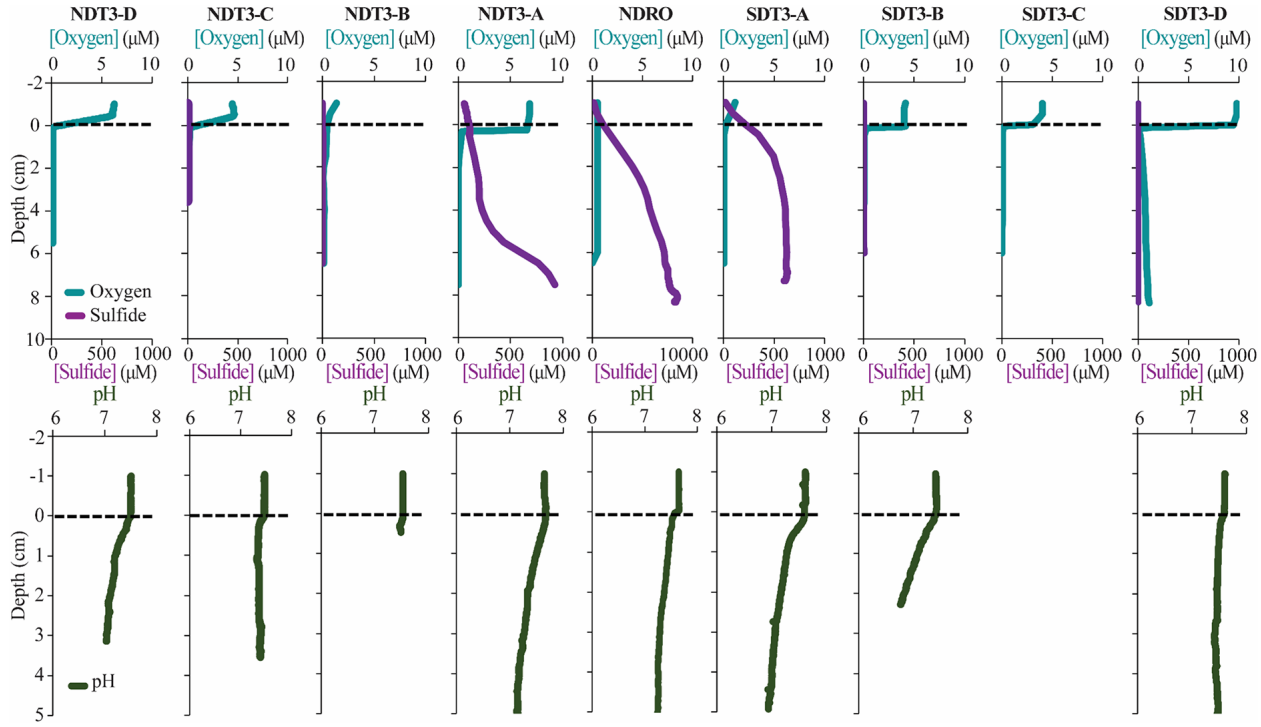

Figure 4. In situ sediment microprofiler results for all stations (except SDT1-A and SDRO): oxygen (O_2) and total sulfide (sulfide) concentration in the first row; pH profiles in the second row. Note the change in scale on the secondary x axis for NDRO sulfide. Values determined in the overlying water are plotted at negative sediment depths; the dotted line connotes the sediment–water interface.

mats in November 2019 fit into this dynamic. For example, mat-forming sulfur bacteria found slightly deeper in the sediment at B stations (see Sect. 4.2) could be progenitors to surface sediment colonization of thick GSOB mats, as has been recorded in other transiently deoxygenated environments (Jørgensen, 1977). Alternatively, these subsurface colonies could also be remnants of a former surface GSOB mat that retreated under changing redox conditions. Oxygenated conditions in the water preceding the 2019 expedition would, in this context, suggest that the mats migrated following a previous anoxic event (Qin et al., 2022). If deoxygenation persisted in the SBB after the AT42-19 cruise, then anitria (i.e., anitric conditions – similar to anoxia) would likely follow in the deepest basin water. These conditions would be similar to those seen in 2013 (Valentine et al., 2016), when GSOB mats formed a contiguous "donut ring" at shallower basin depths. Interestingly, GSOB mats in the eastern Gotland Basin of the Baltic Sea were confined to a hypoxic transition zone, where O_2 was $< 30\,\mu M$ but did not reach anoxia, while no mats were observed at deeper anoxic locations (Noffke et al., 2016). This difference in distribution compared with the SBB suggests that GSOB mats proliferate under different conditions (anoxic or hypoxic), potentially depending on the species of mat-forming bacteria present and whether they specialize in aerobic or anaerobic chemosynthesis.

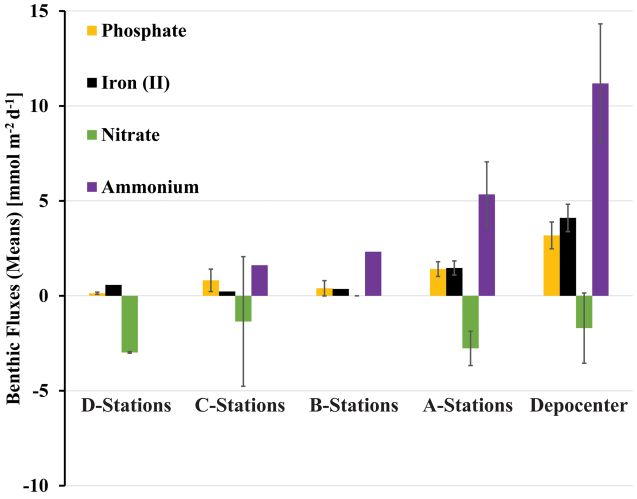

Figure 5. Benthic fluxes of solutes (positive flux: release from the seafloor; negative flux: uptake by the seafloor) determined with in situ benthic flux chambers. Rates were averaged for stations of same depth from the northern and southern transects and the depocenter (NDRO and SDRO). Note that giant sulfur-oxidizing bacterial mats were found at the depocenter and A stations. Error bars represent standard errors.

4.2 Shift from benthic denitrification to dissimilatory nitrate reduction to ammonium in response to complete deoxygenation in the Santa Barbara Basin

Benthic uptake and release of nitrogen species by SBB sediment appeared to be affected by the presence of GSOB mats. While total benthic nitrate uptake was similar between D and depocenter stations based on in situ NO_3^- flux measurements (Fig. 4), NH_4^+ release from the sediment into the water column increased where GSOB mats were present (Fig. 5). This trend is supported by the porewater profiles of NH_4^+, which showed a steeper increase over sediment depth at deeper stations (Figs. 2, 3). Incubations with ^{15}N-NO_3^- revealed that N_2 production (denitrification and anammox) accounted for 86 % of NO_3^- / NO_2^- reduction in the shallow basin, while NH_4^+ production (DNRA) accounted for 13 % and N_2O production accounted for 1 % (NDT3-D; Fig. 6; Peng et al., 2023). In contrast, most (54 %) of the NO_3^- reduction at the depositional center occurred via DNRA; N_2 production accounted for 45 % and N_2O production accounted for 1 % of NO_3^- reduction at SDRO (Fig. 6; Peng et al., 2023). It is important to note that these results only describe patterns of NO_3^- reduction in the basin, while other mechanisms of nitrate uptake by sediment (e.g., hyper-accumulation of nitrate into vacuoles) are more difficult to calculate accurately.

It is likely important to SBB benthic nitrogen cycling that some eukaryotic organisms, including diatoms (Kamp et al., 2011) and foraminifera (Risgaard-Petersen et al., 2006), can hyper-accumulate NO_3^- in benthic, anoxic environments. Additionally, meiofauna (e.g., nematodes) can enhance rates of denitrification (Bonaglia et al., 2014). Both foraminifera and meiofauna were observed in SBB depocenter and A-station sediments in November 2019, and diatoms were observed in shallower sediments in the basin (data not shown). Other studies have found that benthic foraminifera in the SBB depocenter can hyper-accumulate NO_3^- intracellularly up to 375 ± 174 mM (Bernhard et al., 2012) and host symbionts capable of performing denitrification (Bernhard et al., 2000). These foraminifera were found to be responsible for approx. 3 mM N m^{-2} d^{-1}, or 67 % of the total denitrification occurring in the SBB depocenter (Bernhard et al., 2012). Additionally, fungi could reduce NO_3^- or NO_2^- to nitrous oxide in marine sediments and may contribute to denitrification in SBB sediments (Kamp et al., 2015; Lazo-Murphy et al., 2022). This opens up the possibility that the majority of denitrification that we observed in the SBB depocenter is performed by eukaryotes, while prokaryotes (especially GSOB) are responsible for most of the DNRA. The elevated NO_3^- and NO_2^- concentrations observed in our 0–1 cm samples from NDT3-A and SDRO have been reported from SBB depocenter sediments in the past (Reimers et al., 1996; Bernhard et al., 2003) and have been attributed to both GSOB and benthic eukaryotes. The impact of eukaryotes on SBB benthic nitrogen transformation remains to be disentangled from the mats themselves.

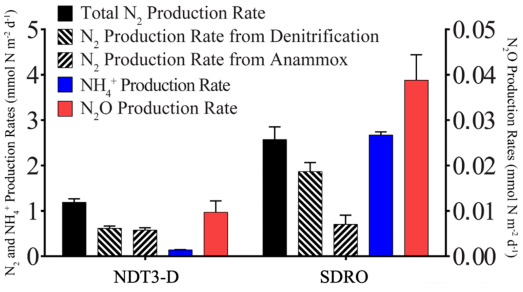

Figure 6. Areal rates of total N_2 production, denitrification, anammox, NH_4^+ production (DNRA), and N_2O production.

Our data suggest a transition from denitrification-dominated sediment in the oxygenated basin to an increasing influence of DNRA on N cycling in the deeper, anoxic basin. Placed in the context of other OMZs, Mauritanian shelf sediment was dominated by denitrification (Dale et al., 2014), similar to SBB shallow sediment (below hypoxic water), while core Peruvian OMZ sediment was dominated by DNRA, similar to sediment of the deeper SBB (below anoxic water) (Sommer et al., 2016). Nitrate reduction in sediment below the seasonally hypoxic Eckernförde Bay (Dale et al., 2011) and below the hypoxic transition zone of the eastern Gotland Basin (Noffke et al., 2016) also showed increased DNRA where GSOB mats were present, although with an NH_4^+ flux (mean of 1.74 mmol m^{-2} d^{-1} and max of 1.10 mmol m^{-2} d^{-1}) that was an order of magnitude lower than that of the SBB depocenter.

While our study suggests a shift from denitrification to DNRA during the deoxygenation of SBB bottom water, other studies have examined changes in benthic nitrogen cycling under reverse conditions, i.e., the reoxidation of the environment following anoxia (Hylén et al., 2022; De Brabandere et al., 2015). After a decadal oxygenation event in the eastern Gotland Basin (Baltic Sea) in 2015–2016, sediment exhibited a slight increase in denitrification but remained dominated by DNRA and N_2O production (Hylén et al., 2022). The lack of N_2 production via denitrification following this oxygenation event was attributed to the reoxygenation event being too weak to substantially oxidize sediments, which would favor denitrification (Hylén et al., 2022). In an engineered reoxygenation event of the By Fjord on Sweden's western coast, where the dissolved O_2 and NO_3^- content of anoxic and anitric bottom water was artificially increased to approx. 130 µM O_2 and 20 µM NO_3^- over a period of roughly 2 years, denitrification rates were increased by an order of magnitude and DNRA rates were also stimulated (De Brabandere et al., 2015). A comparison of our results to these two studies suggests that DNRA bacteria are more resilient to weak reoxygenation events and thrive in transiently deoxygenated systems that remain hypoxic ($O_2 < 63$ µM). The frequency and

magnitude of the reoxygenation and deoxygenation of SBB bottom waters, as well as the effect of these processes on the benthic microbial community, could be a major factor supporting some of the highest recorded total nitrate reduction rates in a natural benthic marine setting (Peng et al., 2023).

A high electron-donor-to-electron-acceptor ratio favors DNRA over denitrification (Marchant et al., 2014; Hardison et al., 2015; Tiedje et al., 1983), and this ratio appears to be critical in determining the dominant nitrate reduction pathway in SBB sediments, similar to the eastern Gotland Basin (Hylén et al., 2022) and the By Fjord (De Brabandere et al., 2015). Example energy yields for denitrification and DNRA are shown in Table 3. As discussed in Tiedje et al. (1983), heterotrophic denitrification yields more energy per mole of electron donor than DNRA. However, the reverse is true when considering the energy yield per mole of electron acceptor (NO_3^-). DNRA also yields three more electrons per molecule of NO_3^- than denitrification. Tiedje et al. (1983) argued that, in environments that are starved of powerful terminal electron acceptors, such as anoxic, organic-rich sediment, the energy yield per electron acceptor and additional electrons available for transfer could push nitrate reduction towards DNRA. Multiple laboratory and model studies have converged on an electron donor to acceptor ratio of approximately 3 to encourage DNRA over denitrification (Hardison et al., 2015; Algar and Vallino, 2014), although other studies have found higher values (Porubsky et al., 2009; Kraft et al., 2014). Sulfide concentrations near the sediment–water interface at the SBB depocenter (approx. 200 µM at 0.5 cm depth, NDRO; Fig. 3) would favor chemoautotrophic DNRA over denitrification at ambient marine nitrate concentrations (approx. 28 µM). Additionally, DNRA appears to be the preferred nitrate reduction pathway for chemoautotrophs that utilize iron or sulfide as an electron donor (Caffrey et al., 2019; Kessler et al., 2019; An and Gardner, 2002). As GSOB mats hyper-accumulate nitrate from the bottom water into their intracellular vacuoles, the resulting decline in electron acceptors at the sediment–water interface coupled with an elevation of the sulfate reduction zone would create an electron-donor-to-electron-acceptor ratio that favors DNRA. As GSOB mats in the SBB seem to prefer DNRA, starving the bottom water of electron acceptors coupled with the high sulfate reduction rates could give them a competitive advantage and allow them to proliferate into the largest (to date) mapped GSOB mat in Earth's oceans, as seen in other expeditions (Valentine et al., 2016; Reimers et al., 1996; Kuwabara et al., 1999).

4.3 Microbial mat proliferation and benthic phosphate remineralization dependent on high rates of organic matter degradation in the Santa Barbara Basin

The organic carbon content of the benthic environment appears to be a key control on sulfate reduction rates near the sediment–water interface as well as microbial mat proliferation. Sulfate reduction rates in the SBB depocenter are most similar in magnitude and profile (i.e., highest rates found at the sediment–water interface and decline drastically thereafter) to those found in sediments below the transiently deoxygenated portion of the Peruvian shelf (e.g., 4.1 mmol m^{-2} d^{-1} at the SBB NDRO station vs. 2.5–3.8 mmol m^{-2} d^{-1} at 128-144 m water depth on the Peruvian margin; Gier et al., 2016; Treude et al., 2021). The TOC content values of surface sediments in these two regions are both high and within the same order of magnitude (maximum recorded TOC of 5.2 % at the 0–1 cm margin at the SDT1-A station compared to 7.6 % in the Peruvian margin at 145 m depth; Noffke et al., 2012). In comparison, sulfate reduction rates in the SBB were at least 1 order of magnitude lower than those found in sediment below the OMZ on the Namibian Shelf, which has much higher TOC contents of > 10 % (Brüchert et al., 2003; Bremner, 1981). Sulfate reduction rates in the shelf sediments below the eastern Arabian OMZ were much lower (0.18–1.27 mmol m^{-2} d^{-1}) than rates in the SBB depocenter (Naik et al., 2017), despite similar hypoxic to anoxic bottom-water conditions. These lower sulfate reduction rates were attributed to the relatively low amount of pelagic primary productivity and, ergo, benthic organic matter delivery in the eastern Arabian OMZ compared with other upwelling systems (Naik et al., 2017). The organic matter content of the sediment appears to be important in the proliferation of GSOB mats; too much TOC could result in toxic levels of sulfide at the sediment–water interface (*Beggiatoa* exhibit an aversion to sulfidic sediments but toxicity has not been quantified) (Preisler et al., 2007), whereas too little sulfide would not provide enough electron donor for the GSOB's chemoautotrophic metabolism.

The profiles of several indicators for benthic anaerobic organic matter remineralization (total alkalinity, DIC, PO_4^{3-}, and NH_4^+) increased in steepness with increasing water depth (Figs. 2a–e, 3a–f). One divergence from this trend can be seen in PO_4^{3-} profiles from the shallow C and D stations, which also featured low rates of sulfate reduction. PO_4^{3-} profiles in these sediments track Fe^{2+} profiles closely; both solutes dip in concentration in areas with visible iron sulfide formation (e.g., 5–11 cm in NDT3-D, as seen in Fig. 2a). Additionally, several stations that exhibited high sulfate reduction rates in surface sediment (e.g., SDT1-A) showed almost no change in PO_4^{3-} at depths below 5 cm (e.g., Fig. 2k–o compared to Fig. 2a–e). This phenomenon has been previously documented in SBB sediment and is attributed to the precipitation of carbonate fluorapatite (Reimers et al.,

Table 3. Example reactions of nitrate reduction pathways with the associated energy yield with respect to the electron donor (H_2 or HS^-) and electron acceptor (NO_3^-) as well as the electron-accepting capacity. Modified from Table 2 in Tiedje et al. (1983).

Reaction	ΔG0' (kcal mol^{-1})		Electrons
	H_2 / HS^-	NO_3^-	per NO_3^-
Chemoheterotrophic denitrification $2NO_3^- + 5H_2 + 2H^+ \rightarrow N_2 + 6H_2O$	−53.6	−133.9	5
Chemoautotrophic denitrification $8NO_3^- + 5HS^- + 3H^+ \rightarrow 5SO_4^{2-} + 4N_2 + 4H_2O$	−177.9	−111.2	5
Chemoheterotrophic DNRA $NO_3^- + 4H_2 + 2H^+ \rightarrow NH_4^+ + 3H_2O$	−35.8	−143.4	8
Chemoautotrophic DNRA $NO_3^- + HS^- + H^+ + H_2O \rightarrow NH_4^+ + SO_4^{2-}$	−107	−107	8

1996). The confinement of these flat PO_4^{3-} profiles to stations with $> 100\,\text{nmol}\,\text{cm}^{-3}\,\text{d}^{-1}$ sulfate reduction in surface sediment suggests that this mineralogical sink of PO_4^{3-} in SBB sediment may be dependent on high sulfate reduction rates, owing to the bicarbonate produced by sulfate reduction (Reimers et al., 1996), and is not found throughout the basin. Flat PO_4^{3-} profiles were also reported from the transiently deoxygenated portion of the Peruvian OMZ, where phosphate mineral precipitation has been documented (Noffke et al., 2012). Similar to the shallow margins of the SBB, PO_4^{3-} in Mauritanian OMZ porewater tracks changes in porewater Fe^{2+} closely (Schroller-Lomnitz et al., 2019), indicating that iron mineralization/dissolution mechanisms have a greater influence on PO_4^{3-} concentrations under hypoxic bottom-water conditions.

4.4 Iron-oxide exhaustion is critical for raising the sulfate reduction zone close to the sediment–water interface in Santa Barbara Basin sediment

The hyper-accumulation of NO_3^- by GSOB mats potentially facilitates sulfate reduction close to the sediment–water interface in the SBB (e.g., NDRO and NDT3-A, as seen in Fig. 2n and o) by starving the sediment of this more powerful electron acceptor. The rise in the sulfate reduction zone at NDT3-C (Fig. 2l) further suggests that the exhaustion of iron oxides and the formation of iron sulfide below the sediment–water interface may play a crucial role in controlling the distribution of sulfate reduction as well. SBB sediments showed a wide vertical and horizontal heterogeneity of redox states based on visual appearance (Fig. 1a–k). Sediment beneath the hypoxic bottom water at the shallowest D stations was reddish, consistent with a high content of iron oxides. Interestingly, porewater Fe^{2+} concentrations in shallower parts of the basin (e.g., NDT3-D, max of $\sim$700 µM Fe^{2+}) were an order of magnitude larger than those found in both the Peruvian (max of $\sim$ 60 and $\sim$ 30 µM Fe^{2+}, respectively; Noffke et al., 2012; Plass et al., 2020) and Mauritanian (max of $\sim$ 50 µM Fe^{2+}; Schroller-Lomnitz et al., 2019) OMZs. It should be noted that porewater samples for geochemical analyses were unfiltered; hence, the reported iron concentrations include aqueous, colloidal, and nanoparticulate species. Regardless, all of these components represent bioavailable sources of iron. Further, as filtering through 0.45 or 0.2 µm filters only removes a fraction of colloidal particles and no nanoparticles (Raiswell and Canfield, 2012), potential surplus porewater iron in SBB samples in comparison to studies that applied filtering was likely minimal.

Deeper in the basin, bands of black sediment that appear mid-core at NDT3-C (6–14 cm) and SDT3-C (6–10 cm) indicate the formation of iron sulfides as a result of sulfide produced by sulfate reduction (Canfield, 1989). Both D stations had similar bottom-water conditions (Table 1), sulfate reduction rates (Figs. 2, 3), porewater concentrations of solutes (Figs. 2, 3), and visual sediment characteristics (Sect. 3.1). On the contrary, there are some noticeable differences in the porewater geochemistry between the two C stations. At the C stations, peaks in sulfate reduction were in the surface sediment, above the iron sulfide layers, and declined below approximately 4 cm, indicating a discrepancy between observed peak sulfate reduction activity and the mineralogical clues left behind by the process. Comparing NDT3-C and SDT3-C, iron sulfide formation (Table 1b compared to Table 1j), porewater Fe^{2+} profiles (Fig. 2g compared to Fig. 3h), and sulfate reduction rates (Fig. 2l compared to Fig. 3n) show that NDT3-C sediment appears to be in transition towards a more sulfidic state, while SDT3-C sediment still mimics the shallow D-station ferruginous state. While sulfate reduction rates for B stations are not available due to technical issues during sample processing, porewater Fe^{2+} profiles show a similar difference between the north and south basin (Fig. 2h compared to Fig. 3i), as did visual sediment characteristics (Table 1c compared to Table 1i). This difference in the biogeochemical profiles and apparent min-

eralogy between the north and south C and B stations could be a result of hydrographic and/or bathymetric differences in the basin (Sholkovitz and Gieskes, 1971; Bograd et al., 2002), but a discernable link between the differences in sediment biogeochemistry and the differences in bottom-water oxygen (Table 1) need to be further explored.

Deeper in the basin (depocenter and A stations), porewater Fe^{2+} concentrations in sediment beneath anoxic bottom water (max of 84 µM Fe^{2+}) were similar to concentrations found below the Peruvian OMZ in 2008 under anoxic bottom-water conditions (78 m water depth, max of 80 µM Fe^{2+}) (Noffke et al., 2012). These deep-basin porewater Fe^{2+} concentrations were, however, an order of magnitude larger than those found at a similar site on the Peruvian shelf (75 m water depth, max of 1 µM Fe^{2+}) in 2017 during a Kelvin-wave-associated "coastal El Niño" event that created oxygenated bottom waters during the sampling and the disappearance of previously observed dense GSOB mats (Plass et al., 2020). As the SBB water column was undergoing rapid deoxygenation in the weeks preceding this study (Qin et al., 2022), the sediments below the sill appeared to be actively shifting from a ferruginous state to a sulfidic state, with this change starting around the C stations and being complete at the depocenter. Comparison of apparent iron sulfide formation with dips in porewater Fe^{2+} concentrations in C-station profiles (Fig. 1b compared to Fig. 2g and Fig. 1j compared to Fig. 3h) signals a shift away from a ferruginous state occurring just below the SBB sill.

C-station porewater Fe^{2+} concentrations and sulfate reduction rates indicate that migration of the sulfate reduction zone towards the sediment–water interface is associated with iron sulfide formation deeper in the sediment. The activity (or lack thereof) of cable bacteria, which are able to bridge the gap between the oxidized sediment–water interface and reduced sediment below using a biofilament (Pfeffer et al., 2012), could explain the interplay between sulfate reduction and iron cycling in SBB sediments. Cable bacteria, such as *Ca.* Electronema sp., contain genes involved in DNRA (Kjeldsen et al., 2019) and can perform nitrate reduction in incubation experiments (Marzocchi et al., 2014), but their direct transformation of NO_3^- in the environment appears limited (Kessler et al., 2019) and they appear to be inactive in anoxic aquatic environments (Seitaj et al., 2015; Marzocchi et al., 2018; Hermans et al., 2019). Cable bacteria primarily conduct aerobic sulfide oxidation (Pfeffer et al., 2012), although they can also utilize Fe^{2+} as an electron donor (Seitaj et al., 2015). The maximum recorded filament length of cable bacteria is 7 cm (Van De Velde et al., 2016), although they are typically not stretched completely vertically through the sediment. The appearance of black sediment in the SBB C-station sediments, starting at approx. 5 cm depth, could be an indication that cable bacteria are oxidizing iron sulfides at that sediment depth and could prevent their formation at shallower depths. Further, cable bacteria have been found to directly compete with GSOB in transiently deoxygenated systems, with cable bacteria active under oxygenated conditions and GSOB active under anoxic conditions (Seitaj et al., 2015). Cable bacteria can also prevent the benthic release of sulfide, which is toxic to many pelagic animals, via the creation of an iron-oxide buffer (formed through Fe^{2+} oxidation) in near-surface sediments (Seitaj et al., 2015). Therefore, if cable bacteria activity in the SBB decreased with declining oxygen concentrations below the sill, the iron-oxide buffer they create could have been reduced, encouraging the sulfate reduction zone to migrate towards the sediment surface (as seen at NDT3-C). Cable bacteria can sometimes be detected in sediments via a slight pH increase (typically pH > 8) (Schauer et al., 2014), which was not reflected in our pH results, but this phenomenon is more typically seen in the laboratory and not the field (Hermans et al., 2019).

4.5 Iron and phosphate flux into SBB bottom water is a feature of transient deoxygenation

The release of dissolved iron and phosphate from sediment below anoxic waters is a well-documented phenomenon (e.g., Mortimer, 1941; Van Cappellen and Ingall, 1994; Van De Velde et al., 2020; Noffke et al., 2012), and this phenomenon is seen in the SBB as well. As postulated previously (Kuwabara et al., 1999), basin flushing oxidizes iron sulfides at the sediment–water interface, providing ample substrate for microbial iron reduction once anoxia returns. This iron reduction initiates high rates of Fe^{2+} release from SBB depocenter sediment (Fig. 5). Iron reduction further releases iron-bound PO_4^{3-} (Mortimer, 1941), as seen by high benthic fluxes of PO_4^{3-} at the depocenter (Fig. 5), although notably some of this PO_4^{3-} release is likely attributed to organic matter degradation (Van Cappellen and Ingall, 1994). High benthic Fe^{2+} and PO_4^{3-} fluxes were also seen on the Peruvian shelf during transient anoxia (Noffke et al., 2012). The release of these solutes was interpreted to be sourced from a layer of reactive iron hydroxides existing near the sediment surface, likely established during a recent oxygenation event. Similar conditions, i.e., visibly oxidized (reddish) sediment laminae and a thin zone of iron reduction apparent from a peak in Fe^{2+} at the sediment–water interface, were found in sediment from the SBB depocenter. Deeper in the persistently anoxic core of the Peruvian OMZ, sediment appears to have little to no flux of Fe^{2+} and PO_4^{3-} into the bottom water (Noffke et al., 2012). Here, iron at the sediment–water interface is hypothesized to be locked up in iron sulfides, which are rarely reoxidized due to persistent anoxia.

In a different study from the eastern Gotland Basin in the Baltic Sea, enhanced elemental fluxes were observed during a decadal oxygen-flushing event (Van De Velde et al., 2020), which was attributed to enhanced elemental recycling (i.e., cycles of mineral precipitation in the water column followed by mineral dissolution once those minerals sink to the sediment). Notably, the iron flux observed in the eastern Gotland Basin (max of 0.08 mmol m^{-2} d^{-1}) (Van De Velde et

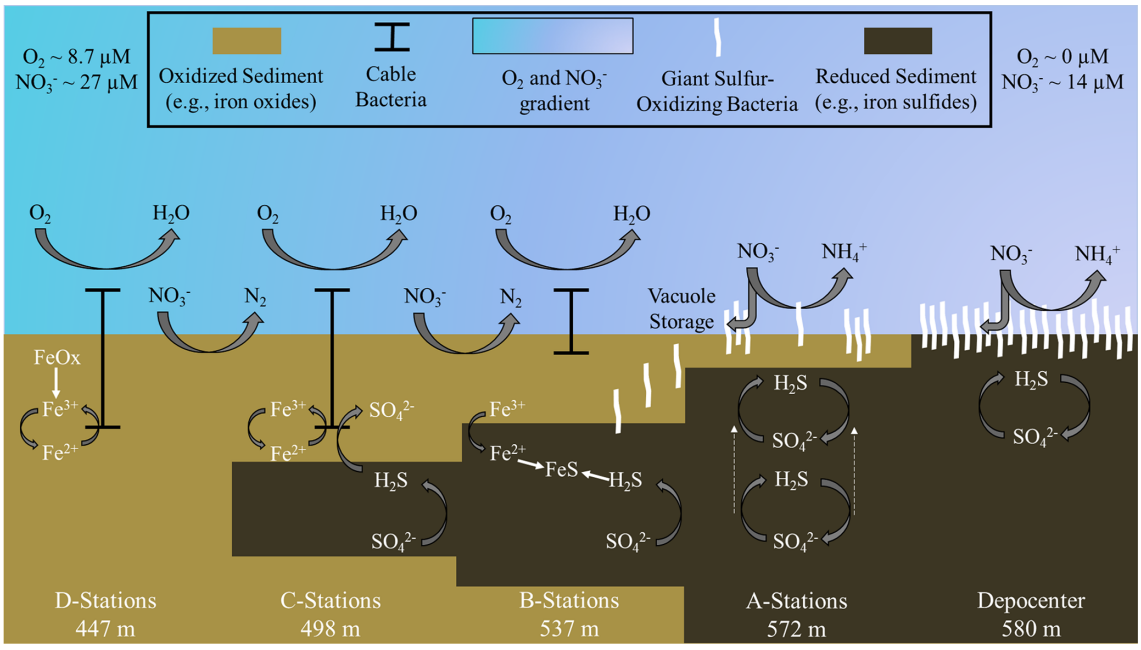

Figure 7. Schematic of biogeochemical processes in the Santa Barbara Basin along the depth gradients studied in October–November 2019. The teal–lavender gradient represents a decline in O_2 and NO_3^- concentrations with basin depth. In the shallower, hypoxic basin (D stations), denitrification and iron reduction are dominant and reduced iron is rapidly reoxidized in near-surface sediment by cable bacteria. Deeper in the basin (A stations and depocenter), nitrogen cycling shifts towards dissimilatory nitrate reduction to ammonia (DNRA). Reduced iron combines with sulfide, produced by sulfate reduction, diffusing from deeper sediment layers to form iron sulfides. As the oxygen concentration approaches zero between the A stations and the basin's depocenter, giant sulfur-oxidizing bacteria hyper-accumulate nitrate in their intracellular vacuoles. Nitrate removal combined with the exhaustion of available iron oxides in the near-surface sediments allows the zone of sulfate reduction to migrate towards the surface (see dashed arrows at A stations), providing the giant sulfur-oxidizing bacteria with sufficient reduced sulfur to proliferate into thick, contiguous mats. Note that the figure is not to scale and that processes are simplified to illustrate the main concepts.

al., 2020) was 2 orders of magnitude lower than the flux observed in the anoxic depocenter of the Santa Barbara Basin (max of 4.9 mmol m^{-2} d^{-1}). It is further notable that benthic fluxes of PO_4^{3-} in the SBB depocenter were also an order of magnitude higher than fluxes in the eastern Gotland Basin's hypoxic transition zone (3.6 vs. 0.23 mmol PO_4^{3-} m^{-2} d^{-1}) (Noffke et al., 2016). These differences in Fe^{2+} and PO_4^{3-} flux between the SBB and the eastern Gotland Basin suggest that reoxidation of the sediment–water interface during basin flushing, as opposed to water-column-associated reoxidation, appears to encourage higher benthic iron fluxes.

Fe^{2+} and PO_4^{3-} fluxes from the SBB depocenter were also approximately 5 times higher (Fig. 5) compared with the anoxic Peruvian shelf (4.9 vs. 0.9 mmol Fe^{2+} m^{-2} d^{-1} and 3.6 vs. 0.8 mmol PO_4^{3-} m^{-2} d^{-1}, respectively) (Noffke et al., 2012). Based on Fe^{2+} profiles, the zone of iron reduction in Peruvian shelf sediments extended down to approx. 10 cm, while the zone appeared to be much shallower and narrower (less than the top 5 cm) in the SBB depocenter. These differences in the magnitude of the Fe^{2+} concentration and Fe^{2+} and PO_4^{3-} flux between the SBB depocenter and the Peruvian shelf could be attributed to differences in the recency and magnitude of reoxygenation events. The release of Fe^{2+} from sediment into the bottom water could create a buffer against reoxygenation in transiently deoxygenated systems, giving a competitive advantage to anaerobic benthic metabolisms (Dale et al., 2013; Wallmann et al., 2022). Additionally, both Fe^{2+} and PO_4^{3-} release from the SBB sediment could allow for higher rates of primary productivity if those constituents diffused into the photic zone (Robinson et al., 2024). The fate of Fe^{2+} and PO_4^{3-} diffusing into SBB waters from the sediment–water interface is a focus of ongoing work within the basin.

5 Conclusions

This research expands upon the wealth of science already conducted in the SBB and other transiently deoxygenated environments by examining changes in benthic biogeochemistry promoted by the onset of anoxia. Our main interpretations are summarized in Fig. 7. We found that GSOB mats proliferate in the SBB where the bottom water is anoxic and nitrate concentrations are declining (A and depocenter stations; Fig. 7). Nitrate uptake by SBB sediment is sim-

ilar regardless of GSOB mat presence, but these mats appear to initiate a shift from denitrification to DNRA as the primary nitrate reduction pathway (beginning at B stations; Fig. 7). The zone of sulfate reduction rises to the sediment–water interface where GSOB mats are present (A stations; Fig. 7), possibly because the hyper-accumulation of nitrate into their intracellular vacuoles starves the environment of this more powerful electron acceptor. However, following the natural order of electron acceptor utilization (Boudreau and Jorgensen, 2001), iron oxides near the sediment–water interface must be exhausted before sulfate reduction can dominate surface sediments and GSOB mats can proliferate in the SBB (depocenter stations; Fig. 7). If anoxic events become longer and more frequent in the SBB because of global warming (see, e.g., Qin et al., 2022; Stramma et al., 2008), the iron-oxide buffer built up at shallower basin depths could be exhausted, allowing for surface sulfate reduction and the proliferation of GSOB mats in shallower margins of the basin than currently seen. Further, the same transient deoxygenation that allows for these mats to reestablish themselves also allows for a high Fe^{2+} and PO_4^{3-} flux into the SBB water column. In order to fully understand the complex changes in the benthic environment in response to deoxygenation, genomic and molecular work of the upper sediment community needs to be characterized. Overall, the insights gleaned from this research will aid in the understanding of fundamental biogeochemical changes that occur when marine environments become anoxic.

Data availability. Biogeochemical data presented in this paper are accessible through the Biological and Chemical Oceanography Data Management Office (BCO-DMO) at https://doi.org/10.26008/1912/bco-dmo.867007.1 (Treude and Valentin, 2022a), https://doi.org/10.26008/1912/bco-dmo.867113.1 (Treude and Valentin, 2022b), https://doi.org/10.26008/1912/bco-dmo.867221.1 (Treude and Valentin, 2022c), and https://doi.org/10.26008/1912/bco-dmo.896706.1 (Treude and Valentin, 2023).

Supplement. The supplement related to this article is available online at: https://doi.org/10.5194/bg-21-789-2024-supplement.

Author contributions. TT, DLV, FK, NL, and JT designed the project. DJY, SJEK, JT, DR, and TT processed sediment cores at sea. DJY conducted geochemical analyses of sediment porewater and benthic flux chamber water. DJY prepared the TOC and TON samples. DR and SJEK analyzed sediment porosity and density. TT and SK performed the shipboard sulfate reduction incubations. DJY and DR conducted the sulfate reduction analyses. DJY, NL, and JT transformed and interpreted the ROV *Jason* data. FJ and FW operated the BFC and microprofilers and analyzed the associated data. XP conducted the ^{15}N experiments and analyses. All authors reviewed and edited the manuscript.

Competing interests. At least one of the (co-)authors is a member of the editorial board of *Biogeosciences*. The peer-review process was guided by an independent editor, and the authors also have no other competing interests to declare.

Disclaimer. Publisher's note: Copernicus Publications remains neutral with regard to jurisdictional claims made in the text, published maps, institutional affiliations, or any other geographical representation in this paper. While Copernicus Publications makes every effort to include appropriate place names, the final responsibility lies with the authors.

Special issue statement. This article is part of the special issue "Low-oxygen environments and deoxygenation in open and coastal marine waters". It is not associated with a conference.

Acknowledgements. We thank the captain, crew, and scientific party of the R/V *Atlantis* and the crew of the ROV *Jason* for their technical and logistical support during the AT42-19 research expedition. We also thank Qianhui Qin, Eleanor Arrington, Molly O'Beirne, Aran Mazariegos, Xiadani Moreno, Alec Eastman, and Kelsey Gosselin for assisting with shipboard analyses. We are grateful to Jiarui Liu for assistance with reviewing the data processing for this paper. We acknowledge Martina Alisch from the Max Planck Institute in Bremen, Germany, for DIC analyses. We also thank Gabriele Eickert-Grötzschel, Vera Hübner, Amja Niclas, Ines Schröder, and Cäcilia Wigand from the Max Planck Institute in Bremen, Germany, for constructing the microsensors. We acknowledge Joy Matthews from the UC Davis Stable Isotope facility for assisting with solid-phase analyses. Funding for this work was provided by the US National Science Foundation, NSF grant nos. OCE-1756947 (to DLV), OCE-1830033 (to DLV), and OCE-1829981 (to TT), and a Simons Foundation Postdoctoral Fellowship in Marine Microbial Ecology (grant no. 547606 to XP). Further support was provided by the Max Planck Society and the Alfred Wegener Institute, Helmholtz Centre for Polar and Marine Research.

Financial support. This research has been supported by the National Science Foundation (grant nos. OCE-1829981, OCE-1830033 and OCE-1756947) and by a Simons Foundation Postdoctoral Fellowship in Marine Microbial Ecology (grant no. 547606).

Review statement. This paper was edited by Caroline P. Slomp and reviewed by two anonymous referees.

References

Algar, C. K. and Vallino, J. J.: Predicting microbial nitrate reduction pathways in coastal sediments, Aquat. Microb. Ecol., 71, 223–238, 2014.

An, S. and Gardner, W. S.: Dissimilatory nitrate reduction to ammonium (DNRA) as a nitrogen link, versus denitrification as a sink in a shallow estuary (Laguna Madre/Baffin Bay, Texas), Mar. Ecol. Prog. Ser., 237, 41–50, 2002.

Bernhard, J. M., Buck, K. R., Farmer, M. A., and Bowser, S. S.: The Santa Barbara Basin is a symbiosis oasis, Nature, 403, 77–80, 2000.

Bernhard, J. M., Visscher, P. T., and Bowser, S. S.: Submillimeter life positions of bacteria, protists, and metazoans in laminated sediments of the Santa Barbara Basin, Limnol. Oceanogr., 48, 813–828, 2003.

Bernhard, J. M., Casciotti, K. L., McIlvin, M. R., Beaudoin, D. J., Visscher, P. T., and Edgcomb, V. P.: Potential importance of physiologically diverse benthic foraminifera in sedimentary nitrate storage and respiration, J. Geophys. Res.-Biogeo., 117, https://doi.org/10.1029/2012JG001949, 2012.

Bograd, S. J., Schwing, F. B., Castro, C. G., and Timothy, D. A.: Bottom water renewal in the Santa Barbara Basin, J. Geophys. Res.-Oceans, 107, 3216, https://doi.org/10.1029/2001JC001291, 2002.

Bonaglia, S., Nascimento, F. A., Bartoli, M., Klawonn, I., and Brüchert, V.: Meiofauna increases bacterial denitrification in marine sediments, Nat. Commun., 5, 5133, https://doi.org/10.1038/ncomms6133, 2014.

Boudreau, B. P. and Jorgensen, B. B.: The benthic boundary layer: Transport processes and biogeochemistry, ISBN 9780195118810, 2001.

Bourbonnais, A., Letscher, R. T., Bange, H. W., Echevin, V., Larkum, J., Mohn, J., Yoshida, N., and Altabet, M. A.: N_2O production and consumption from stable isotopic and concentration data in the Peruvian coastal upwelling system, Global Biogeochem. Cy., 31, 678–698, 2017.

Bremner, J.: Biogenic sediments on the South West African continental margin, https://api.semanticscholar.org/CorpusID:133192933 (last access: 1 February 2024), 1981.

Brüchert, V., Jørgensen, B. B., Neumann, K., Riechmann, D., Schlösser, M., and Schulz, H.: Regulation of bacterial sulfate reduction and hydrogen sulfide fluxes in the central Namibian coastal upwelling zone, Geochim. Cosmochim. Ac., 67, 4505–4518, 2003.

Caffrey, J. M., Bonaglia, S., and Conley, D. J.: Short exposure to oxygen and sulfide alter nitrification, denitrification, and DNRA activity in seasonally hypoxic estuarine sediments, FEMS Microb. Lett., 366, fny288, https://doi.org/10.1093/femsle/fny288, 2019.

Canfield, D. E.: Reactive iron in marine sediments, Geochim. Cosmochim. Ac., 53, 619–632, 1989.

Canfield, D. E., Stewart, F. J., Thamdrup, B., De Brabandere, L., Dalsgaard, T., Delong, E. F., Revsbech, N. P., and Ulloa, O.: A cryptic sulfur cycle in oxygen-minimum–zone waters off the Chilean coast, Science, 330, 1375–1378, 2010.

Charoenpong, C. N., Bristow, L. A., and Altabet, M. A.: A continuous flow isotope ratio mass spectrometry method for high precision determination of dissolved gas ratios and isotopic composition, Limnol. Oceanogr.-Meth., 12, 323–337, 2014.

Cline, J. D.: Spectrophometric determination of hydrogen sulfide in natural waters, Limnol. Oceanogr., 14, 454–458, 1969.

Dale, A. W., Sommer, S., Bohlen, L., Treude, T., Bertics, V. J., Bange, H. W., Pfannkuche, O., Schorp, T., Mattsdotter, M., and Wallmann, K.: Rates and regulation of nitrogen cycling in seasonally hypoxic sediments during winter (Boknis Eck, SW Baltic Sea): Sensitivity to environmental variables, Estuar. Coast. Shelf S., 95, 14–28, 2011.

Dale, A. W., Bertics, V. J., Treude, T., Sommer, S., and Wallmann, K.: Modeling benthic–pelagic nutrient exchange processes and porewater distributions in a seasonally hypoxic sediment: evidence for massive phosphate release by Beggiatoa?, Biogeosciences, 10, 629–651, https://doi.org/10.5194/bg-10-629-2013, 2013.

Dale, A. W., Sommer, S., Ryabenko, E., Noffke, A., Bohlen, L., Wallmann, K., Stolpovsky, K., Greinert, J., and Pfannkuche, O.: Benthic nitrogen fluxes and fractionation of nitrate in the Mauritanian oxygen minimum zone (Eastern Tropical North Atlantic), Geochim. Cosmochim. Ac., 134, 234–256, 2014.

Dale, A. W., Sommer, S., Lomnitz, U., Montes, I., Treude, T., Liebetrau, V., Gier, J., Hensen, C., Dengler, M., Stolpovsky, K., Bryant, L. D., and Wallmann, K.: Organic carbon production, mineralisation and preservation on the Peruvian margin, Biogeosciences, 12, 1537–1559, https://doi.org/10.5194/bg-12-1537-2015, 2015.

Dale, A. W., Sommer, S., Lomnitz, U., Bourbonnais, A., and Wallmann, K.: Biological nitrate transport in sediments on the Peruvian margin mitigates benthic sulfide emissions and drives pelagic N loss during stagnation events, Deep-Sea Res. Pt. I, 112, 123–136, 2016.

De Brabandere, L., Bonaglia, S., Kononets, M. Y., Viktorsson, L., Stigebrandt, A., Thamdrup, B., and Hall, P. O.: Oxygenation of an anoxic fjord basin strongly stimulates benthic denitrification and DNRA, Biogeochemistry, 126, 131–152, 2015.

Emery, K., Hülsemann, J., and Rodolfo, K.: Influence of turbidity currents upon basin waters, Limnol. Oceanogr., 7, 439–446, 1962.

Emmer, E. and Thunell, R. C.: Nitrogen isotope variations in Santa Barbara Basin sediments: Implications for denitrification in the eastern tropical North Pacific during the last 50 000 years, Paleoceanography, 15, 377–387, 2000.

Fossing, H., Gallardo, V. A., Jørgensen, B. B., Hüttel, M., Nielsen, L. P., Schulz, H., Canfield, D. E., Forster, S., Glud, R. N., and Gundersen, J. K.: Concentration and transport of nitrate by the mat-forming sulphur bacterium Thioploca, Nature, 374, 713–715, 1995.

García-Robledo, E., Corzo, A., and Papaspyrou, S.: A fast and direct spectrophotometric method for the sequential determination of nitrate and nitrite at low concentrations in small volumes, Mar. Chem., 162, 30–36, 2014.

Gier, J., Sommer, S., Löscher, C. R., Dale, A. W., Schmitz, R. A., and Treude, T.: Nitrogen fixation in sediments along a depth transect through the Peruvian oxygen minimum zone, Biogeosciences, 13, 4065–4080, https://doi.org/10.5194/bg-13-4065-2016, 2016.

Glud, R. N., Gundersen, J. K., and Ramsing, N. B.: Electrochemical and optical oxygen microsensors for in situ measurements, in: In situ monitoring of aquatic systems: Chemical analysis and speciation, edited by: Buffle, J., and Horvai, G., Wiley, ISBN 0471489794, 2000.

Goericke, R., Bograd, S. J., and Grundle, D. S.: Denitrification and flushing of the Santa Barbara Basin bottom waters, Deep-Sea Res. Pt. II, 112, 53–60, 2015.

Grasshoff, K., Ehrhardt, M., and Kremling, K.: Methods of seawater analysis, Wiley-VCH Verlag GmbH, Weinheim, 632 pp., 1999.

Gundersen, J. K. and Jørgensen, B. B.: Microstructure of diffusive boundary layers and the oxygen uptake of the sea floor, Nature, 345, 604–607, 1990.

Hall, P. O. J. and Aller, R. C.: Rapid small-volume flow injection analysis for SCO_2 and NH_4^+ in marine and fresh waters, Limnol. Oceanogr., 37, 1113–1119, 1992.

Hardison, A. K., Algar, C. K., Giblin, A. E., and Rich, J. J.: Influence of organic carbon and nitrate loading on partitioning between dissimilatory nitrate reduction to ammonium (DNRA) and N_2 production, Geochim. Cosmochim. Ac., 164, 146–160, 2015.

Harris, D., Horwáth, W. R., and Van Kessel, C.: Acid fumigation of soils to remove carbonates prior to total organic carbon or carbon-13 isotopic analysis, Soil Sci. Soc. Am. J., 65, 1853–1856, 2001.

Hermans, M., Lenstra, W. K., Hidalgo-Martinez, S., van Helmond, N. A., Witbaard, R., Meysman, F. J., Gonzalez, S., and Slomp, C. P.: Abundance and biogeochemical impact of cable bacteria in Baltic Sea sediments, Environ. Sci. Technol., 53, 7494–7503, 2019.

Hossain, M., Bhattacharya, P., Frape, S. K., Jacks, G., Islam, M. M., Rahman, M. M., von Brömssen, M., Hasan, M. A., and Ahmed, K. M.: Sediment color tool for targeting arsenic-safe aquifers for the installation of shallow drinking water tubewells, Sci. Total Environ., 493, 615–625, 2014.

Huettel, M., Forster, S., Kloser, S., and Fossing, H.: Vertical migration in the sediment-dwelling sulfur bacteria *Thioploca* spp. in overcoming diffusion limitations, Appl. Environ. Microb., 62, 1863–1872, 1996.

Hylén, A., Bonaglia, S., Robertson, E., Marzocchi, U., Kononets, M., and Hall, P. O.: Enhanced benthic nitrous oxide and ammonium production after natural oxygenation of long anoxic sediments, Limnol. Oceanogr., 67, 419–433, 2022.

Høgslund, S., Revsbech, N. P., Kuenen, J. G., Jørgensen, B. B., Gallardo, V. A., v. d. Vossenberg, J., Nielsen, J. L., Holmkvist, L., Arning, E. T., and Nielsen, L. P.: Physiology and behaviour of marine Thioploca, ISME J., 3, 647–657, 2009.

Jeroschewsky, P., Steuckart, C., and Kuehl, M.: An amperometric microsensor for the determination af H_2S in aquatic environments, Anal. Chem., 68, 4351–4357, 1996.

Jørgensen, B.: Distribution of colorless sulfur bacteria (*Beggiatoa* spp.) in a coastal marine sediment, Mar. Biol., 41, 19–28, 1977.

Jørgensen, B. B.: A comparison of methods for the quantification of bacterial sulphate reduction in coastal marine sediments: I. Measurements with radiotracer techniques, Geomicrobiol. J., 1, 11–27, 1978.

Jørgensen, B. B. and Nelson, D. C.: Sulfide oxidation in marine sediments: Geochemistry meets microbiology, Geol. Soc. Am. Spec. Pap., 379, 63–81, 2004.

Kallmeyer, J., Ferdelman, T. G., Weber, A., Fossing, H., and Jørgensen, B. B.: A cold chromium distillation procedure for radiolabeled sulfide applied to sulfate reduction measurements, Limnol. Oceanogr.-Meth., 2, 171–180, 2004.

Kamp, A., de Beer, D., Nitsch, J. L., Lavik, G., and Stief, P.: Diatoms respire nitrate to survive dark and anoxic conditions, Proceedings of the National Academy of Sciences, 108, 5649–5654, 2011.

Kamp, A., Høgslund, S., Risgaard-Petersen, N., and Stief, P.: Nitrate storage and dissimilatory nitrate reduction by eukaryotic microbes, Fron. Microbiol., 6, 1492, https://doi.org/10.3389/fmicb.2015.01492, 2015.

Kessler, A. J., Wawryk, M., Marzocchi, U., Roberts, K. L., Wong, W. W., Risgaard Petersen, N., Meysman, F. J., Glud, R. N., and Cook, P. L.: Cable bacteria promote DNRA through iron sulfide dissolution, Limnol. Oceanogr., 64, 1228–1238, 2019.

Kjeldsen, K. U., Schreiber, L., Thorup, C. A., Boesen, T., Bjerg, J. T., Yang, T., Dueholm, M. S., Larsen, S., Risgaard-Petersen, N., and Nierychlo, M.: On the evolution and physiology of cable bacteria, P. Natl. Acad. Sci. USA, 116, 19116–19125, 2019.

Kononets, M., Tengberg, A., Nilsson, M., Ekeroth, N., Hylén, A., Robertson, E. K., Van De Velde, S., Bonaglia, S., Rütting, T., and Blomqvist, S.: In situ incubations with the Gothenburg benthic chamber landers: Applications and quality control, J. Mar. Syst., 214, 103475, https://doi.org/10.1016/j.jmarsys.2020.103475, 2021.

Kraft, B., Tegetmeyer, H. E., Sharma, R., Klotz, M. G., Ferdelman, T. G., Hettich, R. L., Geelhoed, J. S., and Strous, M.: The environmental controls that govern the end product of bacterial nitrate respiration, Science, 345, 676–679, 2014.

Kuwabara, J. S., van Geen, A., McCorkle, D. C., and Bernhard, J. M.: Dissolved sulfide distributions in the water column and sediment pore waters of the Santa Barbara Basin, Geochim. Cosmochim. Ac., 63, 2199–2209, 1999.

Lazo-Murphy, B. M., Larson, S., Staines, S., Bruck, H., McHenry, J., Bourbonnais, A., and Peng, X.: Nitrous oxide production and isotopomer composition by fungi isolated from salt marsh sediments, Front. Mar. Sci., 9, 1098508, https://doi.org/10.3389/fmars.2022.1098508, 2022.

Levin, L. A., Gutierrez, D., Rathburn, A. E., Neira, C., Sellanes, J., Munoz, P., Gallardo, V. A., and Salamance, M.: Bethic processes on the Peru margin: a transect across the oxygen minimum zone during the 1997-98 El Nino, Prog. Oceanog., 53, 1–27, 2002.

Marchant, H. K., Lavik, G., Holtappels, M., and Kuypers, M. M.: The fate of nitrate in intertidal permeable sediments, PloS one, 9, e104517, https://doi.org/10.1371/journal.pone.0104517, 2014.

Marzocchi, U., Bonaglia, S., van de Velde, S., Hall, P. O., Schramm, A., Risgaard Petersen, N., and Meysman, F. J.: Transient bottom water oxygenation creates a niche for cable bacteria in long term anoxic sediments of the Eastern Gotland Basin, Environ. Microbiol., 20, 3031–3041, 2018.

Marzocchi, U., Trojan, D., Larsen, S., Louise Meyer, R., Peter Revsbech, N., Schramm, A., Peter Nielsen, L., and Risgaard-Petersen, N.: Electric coupling between distant nitrate reduction and sulfide oxidation in marine sediment, ISME Jo., 8, 1682–1690, 2014.

Middelburg, J. J. and Levin, L. A.: Coastal hypoxia and sediment biogeochemistry, Biogeosciences, 6, 1273–1293, https://doi.org/10.5194/bg-6-1273-2009, 2009.

Mortimer, C. H.: The exchange of dissolved substances between mud and water in lakes, J. Ecol., 29, 280–329, 1941.

Mosch, T., Sommer, S., Dengler, M., Noffke, A., Bohlen, L., Pfannkuche, O., Liebetrau, V., and Wallmann, K.: Factors influencing the distribution of epibenthic megafauna across the Peru-

vian oxygen minimum zone, Deep-Sea Res. Pt. I, 68, 123–135, 2012.

Mußmann, M., Schulz, H. N., Strotmann, B., Kjær, T., Nielsen, L. P., Rosselló Mora, R. A., Amann, R. I., and Jørgensen, B. B.: Phylogeny and distribution of nitrate storing Beggiatoa spp. in coastal marine sediments, Environ. Microbiol., 5, 523–533, 2003.

Myhre, S. E., Pak, D., Borreggine, M., Kennett, J. P., Nicholson, C., Hill, T. M., and Deutsch, C.: Oxygen minimum zone biotic baseline transects for paleoceanographic reconstructions in Santa Barbara Basin, CA, Deep-Sea Res. Pt. II, 150, 118–131, 2018.

Naik, R., Naqvi, S., and Araujo, J.: Anaerobic carbon mineralisation through sulphate reduction in the inner shelf sediments of eastern Arabian Sea, Estuar. Coast., 40, 134–144, 2017.

Noffke, A., Sommer, S., Dale, A., Hall, P., and Pfannkuche, O.: Benthic nutrient fluxes in the Eastern Gotland Basin (Baltic Sea) with particular focus on microbial mat ecosystems, J. Mar. Syst., 158, 1–12, 2016.

Noffke, A., Hensen, C., Sommer, S., Scholz, F., Bohlen, L., Mosch, T., Graco, M., and Wallmann, K.: Benthic iron and phosphorus fluxes across the Peruvian oxygen minimum zone, Limnol. Oceanogr., 57, 851–867, 2012.

Pavlova, G. Y., Tishchenko, P. Y., Volkova, T., Dickson, A., and Wallmann, K.: Intercalibration of Bruevich's method to determine the total alkalinity in seawater, Oceanology, 48, 438–443, 2008.

Peng, X., Ji, Q., Angell, J. H., Kearns, P. J., Yang, H. J., Bowen, J. L., and Ward, B. B.: Long term fertilization alters the relative importance of nitrate reduction pathways in salt marsh sediments, J. Geophys. Res.-Biogeo., 121, 2082–2095, 2016.

Peng, X., Yousavich, D. J., Bourbonnais, A., Wenzhoefer, F., Janssen, F., Treude, T., and Valentine, D. L.: The fate of fixed nitrogen in Santa Barbara Basin sediments during seasonal anoxia, EGUsphere [preprint], https://doi.org/10.5194/egusphere-2023-1498, 2023.

Pfeffer, C., Larsen, S., Song, J., Dong, M., Besenbacher, F., Meyer, R. L., Kjeldsen, K. U., Schreiber, L., Gorby, Y. A., and El-Naggar, M. Y.: Filamentous bacteria transport electrons over centimetre distances, Nature, 491, 218–221, 2012.

Plass, A., Schlosser, C., Sommer, S., Dale, A. W., Achterberg, E. P., and Scholz, F.: The control of hydrogen sulfide on benthic iron and cadmium fluxes in the oxygen minimum zone off Peru, Biogeosciences, 17, 3685–3704, https://doi.org/10.5194/bg-17-3685-2020, 2020.

Porubsky, W., Weston, N., and Joye, S.: Benthic metabolism and the fate of dissolved inorganic nitrogen in intertidal sediments, Eastuar. Coast. Shelf S., 83, 392–402, 2009.

Preisler, A., De Beer, D., Lichtschlag, A., Lavik, G., Boetius, A., and Jørgensen, B. B.: Biological and chemical sulfide oxidation in a Beggiatoa inhabited marine sediment, ISME J., 1, 341–351, 2007.

Prokopenko, M., Hammond, D., Berelson, W., Bernhard, J., Stott, L., and Douglas, R.: Nitrogen cycling in the sediments of Santa Barbara basin and Eastern Subtropical North Pacific: Nitrogen isotopes, diagenesis and possible chemosymbiosis between two lithotrophs (Thioploca and Anammox) – "riding on a glider", Earth Planet. Sc. Lett., 242, 186–204, 2006.

Qin, Q., Kinnaman, F. S., Gosselin, K. M., Liu, N., Treude, T., and Valentine, D. L.: Seasonality of Water Column Methane Oxidation and Deoxygenation in a Dynamic Marine Environment, Geochim. Cosmochim. Ac., 336, 219–230, https://doi.org/10.1016/j.gca.2022.09.017, 2022.

Raiswell, R. and Canfield, D. E.: The iron biogeochemical cycle past and present, Geochem. Perspec., 1, 1–2, 2012.

Reimers, C. E., Ruttenberg, K. C., Canfield, D. E., Christiansen, M. B., and Martin, J. B.: Porewater pH and authigenic phases formed in the uppermost sediments of Santa Barbara Basin, Geochim. Cosmochim. Acta, 60, 4037–4057, 1996.

Revsbech, N. P. and Jørgensen, B. B.: Microelectrodes: their use in microbial ecology, edited by: Marshall, K. C., Adv. Microb. Ecol., 9, 293–352, https://doi.org/10.1007/978-1-4757-0611-6_7, 1986.

Risgaard-Petersen, N., Langezaal, A. M., Ingvardsen, S., Schmid, M. C., Jetten, M. S. M., Op den Camp, H. J. M., Derksen, J. W. M., Pina-Ochoa, E., Eriksson, S. P., Nielsen, L. P., Revsbech, N. P., Cedhagen, T., and Zwaan van der, G. J.: Evidence for complete denitrification in a benthic foraminifer, Nature, 443, 93–96, 2006.

Robinson, D., Pham, A. L. D., Yousavich, D. J., Janssen, F., Wenzhöfer, F., Arrington, E. C., Gosselin, K. M., Sandoval-Belmar, M., Mar, M., Valentine, D. L., Bianchi, D., and Treude, T.: Iron "ore" nothing: benthic iron fluxes from the oxygen-deficient Santa Barbara Basin enhance phytoplankton productivity in surface waters, Biogeosciences, 21, 773–788, https://doi.org/10.5194/bg-21-773-2024, 2024.

Sayama, M.: Presence of nitrate-accumulating sulfur bacteria and their influence on nitrogen cycling in a shallow coastal marine sediment, Appl. Environ. Microb., 67, 3481–3487, 2001.

Schauer, R., Risgaard-Petersen, N., Kjeldsen, K. U., Tataru Bjerg, J. J., B Jørgensen, B., Schramm, A., and Nielsen, L. P.: Succession of cable bacteria and electric currents in marine sediment, ISME J., 8, 1314–1322, 2014.

Schroller-Lomnitz, U., Hensen, C., Dale, A. W., Scholz, F., Clemens, D., Sommer, S., Noffke, A., and Wallmann, K.: Dissolved benthic phosphate, iron and carbon fluxes in the Mauritanian upwelling system and implications for ongoing deoxygenation, Deep-Sea Res. Pt. I, 143, 70–84, 2019.

Schulz, H. N. and Schulz, H. D.: Large sulfur bacteria and the formation of phosphorite, Science, 307, 416–418, 2005.

Schulz, H. N., Jorgensen, B. B., Fossing, H. A., and Ramsing, N. B.: Community structure of filamentous, sheath-building sulfur bacteria, *Thioploca* spp., off the coast of Chile, Appl. Environ. Microb., 62, 1855–1862, 1996.

Schulz, H. N., Brinkhoff, T., Ferdelman, T. G., Hernández Mariné, M., Teske, A., and Jørgensen, B. B.: Dense populations of a giant sulfur bacterium in Namibian shelf sediments, Science, 284, 493–495, 1999.

Seitaj, D., Schauer, R., Sulu-Gambari, F., Hidalgo-Martinez, S., Malkin, S. Y., Burdorf, L. D., Slomp, C. P., and Meysman, F. J.: Cable bacteria generate a firewall against euxinia in seasonally hypoxic basins, P. Natl. Acad. Sci. USA, 112, 13278–13283, 2015.

Sholkovitz, E.: Interstitial water chemistry of the Santa Barbara Basin sediments, Geochim. Cosmochim. Ac., 37, 2043-2073, 1973.

Sholkovitz, E. R. and Gieskes, J. M.: A Physical chemical study of the flushing of the santa barbara basin[1], Limnol. Oceanogr., 16, 479–489, 1971.

Sigman, D. M., Robinson, R., Knapp, A., Van Geen, A., McCorkle, D., Brandes, J., and Thunell, R.: Distinguishing between water column and sedimentary denitrification in the Santa Barbara Basin using the stable isotopes of nitrate, Geochem. Geophy. Geosy., 4, https://doi.org/10.1029/2002GC000384, 2003.

Sommer, S., Gier, J., Treude, T., Lomnitz, U., Dengler, M., Cardich, J., and Dale, A. W.: Depletion of oxygen, nitrate and nitrite in the Peruvian oxygen minimum zone cause an imbalance of benthic nitrogen fluxes, Deep-Sea Res. Pt. I, 112, 113–122, 2016.

Stramma, L., Johnson, G. C., Sprintall, J., and Mohrholz, V.: Expanding oxygen-minimum zones in the tropical oceans, Science, 320, 655–658, 2008.

Sverdrup, H. and Allen, W.: Distribution of diatoms in relation to the character of water masses and currents off Southern California in 1938, J. Mar. Res., 2, 131–144, 1939.

Thunell, R. C.: Particle fluxes in a coastal upwelling zone: sediment trap results from Santa Barbara Basin, California, Deep-Sea Res. Pt. II, 45, 1863–1884, 1998.

Tiedje, J. M., Sexstone, A. J., Myrold, D. D., and Robinson, J. A.: Denitrification: ecological niches, competition and survival, Antonie van Leeuwenhoek, 48, 569–583, 1983.

Treude, T.: Biogeochemical reactions in marine sediments underlying anoxic water bodies, in: Anoxia: Paleontological Strategies and Evidence for Eukaryote Survival, edited by: Altenbach, A., Bernhard, J., and Seckbach, J., Cellular Origins, Life in Extreme Habitats and Astrobiology (COLE) Book Series, Springer, Dordrecht, 18–38, 2011.

Treude, T., Smith, C. R., Wenzhoefer, F., Carney, E., Bernardino, A. F., Hannides, A. K., Krueger, M., and Boetius, A.: Biogeochemistry of a deep-sea whale fall: sulfate reduction, sulfide efflux and methanogenesis, Mar. Ecol. Prog. Ser., 382, 1–21, 2009.

Treude, T., Hamdan, L. J., Lemieux, S., Dale, A. W., and Sommer, S.: Rapid sulfur cycling in sediments from the Peruvian oxygen minimum zone featuring simultaneous sulfate reduction and sulfide oxidation, Limnol. Oceanogr., 66, 2661–2671, 2021.

Treude, T. and Valentine, D. L.: Porewater geochemistry of sediments collected Fall 2019 in the Santa Barbara Basin using ROV *Jason* during R/V *Atlantis* cruise AT42-19 (Version 1) [data set], Biological and Chemical Oceanography Data Management Office (BCO-DMO). https://doi.org/10.26008/1912/BCO-DMO.867007.1, 2022a.

Treude, T. and Valentine, D. L.: Porosity and density of sediments collected Fall 2019 in the Santa Barbara Basin using ROV *Jason* during R/V *Atlantis* cruise AT42-19 (Version 1) [data set], Biological and Chemical Oceanography Data Management Office (BCO-DMO). https://doi.org/10.26008/1912/BCO-DMO.867113.1, 2022b.

Treude, T. and Valentine, D. L.: Microbial activity from sediments collected Fall 2019 in the Santa Barbara Basin using ROV *Jason* during R/V *Atlantis* cruise AT42-19 (Version 1) [data set], Biological and Chemical Oceanography Data Management Office (BCO-DMO). https://doi.org/10.26008/1912/BCO-DMO.867221.1, 2022c.

Treude, T. and Valentine, D. L.: Benthic fluxes of solutes measured by in-situ benthic flux chambers along two depth transects in the Santa Barbara Basin during November 219 (Version 1) [data Set], Biological and Chemical Oceanography Data Management Office (BCO-DMO). https://doi.org/10.26008/1912/bco-dmo.896706.1, 2023.

Valentine, D. L., Fisher, G. B., Pizarro, O., Kaiser, C. L., Yoerger, D., Breier, J. A., and Tarn, J.: Autonomous marine robotic technology reveals an expansive benthic bacterial community relevant to regional nitrogen biogeochemistry, Environ. Sci. Technol., 50, 11057–11065, 2016.

Van Cappellen, P. and Ingall, E. D.: Benthic phosphorus regeneration, net primary production, and ocean anoxia: A model of the coupled marine biogeochemical cycles of carbon and phosphorus, Paleoceanography, 9, 677–692, 1994.

Van De Velde, S., Lesven, L., Burdorf, L. D., Hidalgo-Martinez, S., Geelhoed, J. S., Van Rijswijk, P., Gao, Y., and Meysman, F. J.: The impact of electrogenic sulfur oxidation on the biogeochemistry of coastal sediments: A field study, Geochim. Cosmochim. Ac., 194, 211–232, 2016.

van de Velde, S. J., Hylén, A., Kononets, M., Marzocchi, U., Leermakers, M., Choumiline, K., Hall, P. O., and Meysman, F. J.: Elevated sedimentary removal of Fe, Mn, and trace elements following a transient oxygenation event in the Eastern Gotland Basin, central Baltic Sea, Geochim. Cosmochim. Ac., 271, 16–32, 2020.

van de Velde, S. J., Hylén, A., Eriksson, M., James, R. K., Kononets, M. Y., Robertson, E. K., and Hall, P. O.: Exceptionally high respiration rates in the reactive surface layer of sediments underlying oxygen-deficient bottom waters, P. Roy. Soc. A-Math. Phy., 479, 20230189, https://doi.org/10.1098/rspa.2023.0189, 2023.

Wallmann, K., José, Y. S., Hopwood, M. J., Somes, C. J., Dale, A. W., Scholz, F., Achterberg, E. P., and Oschlies, A.: Biogeochemical feedbacks may amplify ongoing and future ocean deoxygenation: a case study from the Peruvian oxygen minimum zone, Biogeochemistry, 159, 45–67, 2022.

Ward, B., Devol, A., Rich, J., Chang, B., Bulow, S., Naik, H., Pratihary, A., and Jayakumar, A.: Denitrification as the dominant nitrogen loss process in the Arabian Sea, Nature, 461, 78–81, 2009.

Zhang, L., Altabet, M. A., Wu, T., and Hadas, O.: Sensitive measurement of $NH_4 + {}^{15}N/{}^{14}N$ ($\delta^{15}NH_4^+$) at natural abundance levels in fresh and saltwaters, Anal. Chem., 79, 5297–5303, 2007.

Zopfi, J., Kjær, T., Nielsen, L. P., and Jørgensen, B. B.: Ecology of *Thioploca* spp.: nitrate and sulfur storage in relation to chemical microgradients and influence of Thioploca spp. on the sedimentary nitrogen cycle, Appl. Environ. Microb., 67, 5530–5537, 2001.